Author Manuscript

Author Manuscript

Author Manuscript

Author Manuscript

HHS Public Access

Author manuscript

Neurobiol Dis. Author manuscript; available in PMC 2021 February 01.

Published in final edited form as:

Neurobiol Dis. 2020 February ; 134: 104638. doi:10.1016/j.nbd.2019.104638.

Decreased number of striatal cholinergic interneurons and motor deficits in dopamine receptor 2-expressing-cell-specific *Dyt1* conditional knockout mice

Fumiaki Yokoi[a,*], **Janneth Oleas**[a], **Hong Xing**[a], **Yuning Liu**[a], **Kelly M. Dexter**[a], **Carly Misztal**[a], **Melinda Gerard**[a], **Iakov Efimenko**[a], **Patrick Lynch**[a], **Matthew Villanueva**[a], **Raul Alsina**[a], **Shiv Krishnaswamy**[a], **David E. Vaillancourt**[b,c,d], **Yuqing Li**[a,*]

[a]Norman Fixel Institute for Neurological Diseases, Department of Neurology, College of Medicine, University of Florida, Gainesville, Florida, 32610-0236, United States of America

[b]Laboratory for Rehabilitation Neuroscience, Department of Applied Physiology and Kinesiology, University of Florida, Gainesville, Florida, 32611-8205, United States of America

[c]J. Crayton Pruitt Family Department of Biomedical Engineering, University of Florida, Gainesville, Florida, 32611-8205, United States of America

[d]Department of Neurology and Center for Movement Disorders and Neurorestoration, College of Medicine, University of Florida, Gainesville, Florida, 32611-8205, United States of America

Abstract

DYT1 early-onset generalized torsion dystonia is a hereditary movement disorder characterized by abnormal postures and repeated movements. It is caused mainly by a heterozygous trinucleotide deletion in *DYT1/TOR1A*, coding for torsinA. The mutation may lead to a partial loss of torsinA function. Functional alterations of the basal ganglia circuits have been implicated in this disease. Striatal dopamine receptor 2 (D2R) levels are significantly decreased in DYT1 dystonia patients and in the animal models of DYT1 dystonia. D2R-expressing cells, such as the medium spiny neurons in the indirect pathway, striatal cholinergic interneurons, and dopaminergic neurons in the basal ganglia circuits, contribute to motor performance. However, the function of torsinA in these neurons and its contribution to the motor symptoms is not clear. Here, D2R-expressing-cell-specific *Dyt1* conditional knockout (d2KO) mice were generated and *in vivo* effects of torsinA loss in the corresponding cells were examined. The *Dyt1* d2KO mice showed significant reductions of striatal torsinA, acetylcholine metabolic enzymes, Tropomyosin receptor kinase A (TrkA), and cholinergic interneurons. The *Dyt1* d2KO mice also showed significant reductions of striatal D2R dimers and tyrosine hydroxylase without significant alteration in striatal monoamine contents or the number of dopaminergic neurons in the substantia nigra. The *Dyt1* d2KO male

[*]Corresponding authors at: Department of Neurology, College of Medicine, University of Florida, PO Box 100236, Gainesville, FL 32610-0236, USA. fumiaki.yokoi@neurology.ufl.edu, yuqingli@ufl.edu.

Conflict of Interest statement

The authors declare no competing financial interests.

Publisher's Disclaimer: This is a PDF file of an unedited manuscript that has been accepted for publication. As a service to our customers we are providing this early version of the manuscript. The manuscript will undergo copyediting, typesetting, and review of the resulting proof before it is published in its final form. Please note that during the production process errors may be discovered which could affect the content, and all legal disclaimers that apply to the journal pertain.

Author Manuscript Author Manuscript Author Manuscript Author Manuscript

mice showed motor deficits in the accelerated rotarod and beam-walking tests without overt dystonic symptoms. Moreover, the *Dyt1* d2KO male mice showed significant correlations between striatal monoamines and locomotion. The results suggest that torsinA in the D2R-expressing cells play a critical role in the development or survival of the striatal cholinergic interneurons, expression of striatal D2R mature form, and motor performance. Medical interventions to compensate for the loss of torsinA function in these neurons may affect the onset and symptoms of this disease.

Keywords

beam walking; cholinergic interneuron; dopamine; *Drd2-Cre*; dystonia; DYT1; torsinA; *TOR1A*; TrkA; vesicular acetylcholine transporter

1. Introduction

DYT1 early-onset generalized dystonia (dystonia 1: OMIM: #128100) is an inherited movement disorder characterized by abnormal torsion postures and involuntary repeated movements (Albanese et al., 2013; Breakefield et al., 2008). The onset of this disease occurs during either childhood or adolescence. The symptoms usually start in the legs and extend to the upper body. A heterozygous in-frame trinucleotide deletion (ΔGAG) mutation in *DYT1/TOR1A*, which causes a glutamic acid loss in the C-terminal region of torsinA, was initially identified in these patients (Ozelius et al., 1997). The penetrance of this disease is 30–40%.Although most of the DYT1 dystonia patients have the ΔGAG mutation, other mutations in the gene have also been reported (Calakos et al., 2010; Doheny et al., 2002; Eidelberg et al., 1998; Grusser-Cornehls et al., 1999; Leung et al., 2001; Mandavilli et al., 2000; Ritz, 2009). Moreover, a homozygous nonsense mutation in *DYT1/TOR1A* was found in a two-month-old boy with severe arthrogryposis, developmental delay and dystonic movements (Isik et al., 2018). Although most patients have the heterozygous ΔGAG mutation, the existence of multiple other mutations including the nonsense mutations in some patients suggest that partial loss of torsinA function may lead to the dystonic symptoms. Deep brain stimulation targeting the globus pallidus internus ameliorates dystonic symptoms (Cif et al., 2010), suggesting a functional alteration of the basal ganglia circuits in this disease. Trihexyphenidyl (THP), an antagonist of muscarinic acetylcholine receptors, is commonly used to treat dystonic symptoms in humans (Jankovic, 2006), suggesting an impairment of the cholinergic system or its related circuits in this disease (Eskow Jaunarajs et al., 2015).

Dyt1 ΔGAG heterozygous knock-in (KI) mice, which have the corresponding trinucleotide deletion mutation in the endogenous *Dyt1*/*Tor1a*, exhibit the long-term depression (LTD) deficits in the corticostriatal pathway (Dang et al., 2012). These mice show sustained contraction and co-contraction of agonist and antagonist muscles of the hind limbs (DeAndrade et al., 2016), and motor deficits of the hind limbs in the beam-walking test (Dang et al., 2005). These symptoms were ameliorated by THP treatment. The motor deficits in the beam-walking test were reproduced in distinct batches of the *Dyt1* KI mouse line (Cao et al., 2010; Yokoi et al., 2012a) and in another line of ΔGAG KI mice of torsinA

Author Manuscript Author Manuscript Author Manuscript Author Manuscript

(Song et al., 2012), suggesting that the motor deficits were reproducible in these independent KI lines. Furthermore, transgenic mouse overexpressing human mutant (ΔGAG) torsinA from human cytomegalovirus (CMV) immediate early promoter (hMT mouse) also show LTD deficits in the corticostriatal pathway (Martella et al., 2009) and motor learning deficits in the accelerating rotarod test (Sharma et al., 2005). Recovery of LTD deficits in the corticostriatal pathway by THP treatment was also confirmed in another line of ΔGAG KI mice (Maltese et al., 2014).

Dyt1 heterozygous knock-out (KO) mice (Yokoi et al., 2015a), *Dyt1* knock-down (KD) mice (Dang et al., 2006), the cerebral cortex-specific *Dyt1* conditional KO (Yokoi et al., 2008), striatum-specific *Dyt1* conditional KO (Yokoi et al., 2011), and cholinergic cell-specific *Dyt1* conditional KO mice (Sciamanna et al., 2012) exhibit motor deficits. Furthermore, an N-CKO mouse model, which contains a heterozygous KO in one allele and *Nestin-cre*-mediated heterozygous conditional KO of *Dyt1*/*Tor1a* exons 3–5 in another allele, exhibits weak walking, abnormal twisting, and complete postnatal lethality (Liang et al., 2014). A forebrain-specific conditional KO mouse model of torsinA (Dlx-CKO mice), which has a combination of a heterozygous KO in one allele and Dlx-cre-derived forebrain-specific conditional KO of the exons 3–5 in another allele, show neurodegeneration of the striatal cholinergic interneurons (ChIs), growth retardation, severe motor symptoms and complete lethality before weaning age (Pappas et al., 2015). ChAT-CKO mice, which have a heterozygous *Tor1a*/*Dyt1* KO in one allele and *ChAT-cre*-mediated heterozygous conditional KO of the exons 3–5 in another allele, also show motor deficits (Pappas et al., 2018). Finally, null-mutation of the X-linked dtrosin, an ortholog of the *DYT1*/ *TOR1A*, in a fly model show semi-lethality, locomotion defects, reductions of GTP cyclohydrolase and dopamine (Wakabayashi-Ito et al., 2011). These models suggest that partial loss of torsinA function may contribute to motor deficits. On the other hand, mouse models overexpressing human torsinA in wild-type (WT) and mutant form using murine prion promoter exhibit abnormal motor performance in beam-walking test (Grundmann et al., 2007), suggesting that a precise expression level of torsinA in appropriate cells is important for fine motor coordination although a possibility that ectopic expression of a protein from different species affects motor function is not excluded.

The ΔGAG mutation causes a reduction of the brain tissue torsinA level in both lines of *Dyt1* KI mice (Goodchild et al., 2005; Yokoi et al., 2010). Consistently, torsinA levels are reduced in the fibroblasts from a DYT1 dystonia patient with the ΔGAG mutation (Goodchild et al., 2005). Other *in vitro* studies using the cultured cells expressing the mutant torsinA suggest that the mutant torsinA is not stable in the cells (Giles et al., 2008; Gordon and Gonzalez- Alegre, 2008). Moreover, electrophysiological properties of the hippocampi in both KI and heterozygous KO mice showed similar neurotransmitter releasing deficits (Yokoi et al., 2013; Yokoi et al., 2015a). These studies suggest that ΔGAG mutation is a loss of function mutation both *in vitro* and *in vivo*.

A postmortem analysis in a DYT1 dystonia patient brain suggested reduced dopamine in rostral portions of the putamen and caudate nucleus (Furukawa et al., 2000). Another postmortem study reported increased striatal 3,4-dihydroxyphenylacetic acid (DOPAC)/ dopamine ratio and trends of decreased striatal binding activities of [^{3}H]SCH-23390 radio-

Author Manuscript Author Manuscript Author Manuscript Author Manuscript

ligand to dopamine receptor 1 (D1R) and [^{3}H]YM-09151–2 radio-ligand to dopamine receptor 2 (D2R) (Augood et al., 2002). A positron emission tomography study suggested that striatal D2R availability is reduced in both manifesting and non-manifesting DYT1 mutation carriers (Asanuma et al., 2005). *Dyt1* KI male mice exhibit a reduced homovanillic acid (HVA) level in the striatum (Dang et al., 2005), and *Dyt1* KD mice show a decreased level of striatal DOPAC (Dang et al., 2006). A transgenic mouse model, which overexpresses human mutant torsinA with the CMV promoter, shows a reduction of striatal D2R (Napolitano et al., 2010). Consistently, striatal D2R levels are significantly reduced in both the *Dyt1* KI and striatum-specific *Dyt1* conditional KO mice (Dang et al., 2012; Yokoi et al., 2011). Striatal D1R levels are also significantly reduced in *Dyt1* KI mice (Yokoi et al., 2015b). D2R-expressing cells, such as the medium spiny neurons (MSNs) in the indirect pathway, striatal ChIs, and dopaminergic neurons in the basal ganglia circuits, are known to contribute to motor coordination and learning. Since phasic late excitation in the substantia nigra through the striatopallidal indirect pathway plays a role in stopping movements (Sano et al., 2013), malfunction of the indirect pathway may contribute to hyperkinetic disorders such as dystonia. Reductions of striatal D2R in both patients and animal models suggest that D2R-expressing neurons in the basal ganglia circuits may contribute to DYT1 dystonia. However, the function of torsinA in these neurons and its contribution to the motor symptoms in this disease are not clear. Here, a novel D2R- expressing-cell-specific *Dyt1* conditional KO (*Dyt1* d2KO) mouse model was generated to examine the *in vivo* effect of torsinA loss in the D2R-expressing neurons.

2. Materials and methods

2.1. Animals

All animal experiments were conducted in compliance with the USPHS Guide for Care and Use of Laboratory Animals and approved by the Institutional Animal Use and Care Committee at the University of Florida. *Drd2-Cre* mice were purchased from MMRRC (Cat. No. 032108; B6.FVB(Cg)-Tg(Drd2-cre)ER44Gsat/Mmucd) (Gong et al., 2007). *Dyt1 loxP* mice, which have floxed exons 3–4 in *Dyt1*, were prepared as previously described (Yokoi et al., 2008). *Drd2-Cre* +/− *Dyt1 loxP* +/− (double heterozygote: DHet) was generated by crossing the *Drd2-Cre* +/− mice and either heterozygous *Dyt1 loxP* +/− or homozygous *Dyt1 loxP* −/− mice (had both copies of loxP sequences). *Dyt1* d2KO mice were generated by crossing the DHet mice and either *Dyt1 loxP* +/− or *Dyt1 loxP* −/− mice. Genotyping was performed by using PCR with tail DNA at two to three weeks old and specific primers for *Drd2-Cre* and *Dyt1 loxP*. The number of pups in each genotype were compared to analyze the neonatal lethality of the *Dyt1* d2KO mice. Mice were housed with *ad libitum* access to food and water under the condition of 12 hours of light and 12 hours of dark.

2.2. Western blot analysis

Antibodies used for Western blot analysis and fluorescence immunohistochemistry (FIHC) are listed in Appendix Table A.1. The striata were dissected from the *Dyt1* d2KO (n = 8) and control littermate (CT; *Dyt1 loxP* +/−: n = 1; *Dyt1 loxP* −/−: n = 5) male mice at 91–135 days- old and homogenized in 200 μl of ice-cold lysis buffer and proteins were extracted in 1% Triton X-100 in the buffer as previously described (Yokoi et al., 2010). Protein samples

Author Manuscript Author Manuscript Author Manuscript Author Manuscript

were separated on SDS-polyacrylamide gel electrophoresis with Precision Plus Protein All Blue Prestained Protein standards (BIO-RAD; #1610373). The proteins were transferred on the Millipore Immobilon-FL PVDF membrane. The expression levels of torsinA, D2R, DARPP-32, p-DARPP- 32, choline acetyltransferase (ChAT), vesicular acetylcholine transporter (VAChT), choline transporter (ChT), acetylcholinesterase (AChE), TrkA, and tyrosine hydroxylase (TH) were measured and normalized with the expression level of glyceraldehyde-3-phosphate dehydrogenase (GAPDH) or β-tubulin. The secondary antibodies with LI-COR IRDye were used as appropriate. The infrared emission signals were detected and recorded as digital data by an LI-COR Odyssey imaging system. All Western blot data used in this manuscript were not saturated. The molecular weight of each protein was estimated by comparing the migration distance of the corresponding band with the protein standards.

2.3. Fluorescence immunohistochemistry

Dyt1 d2KO (n=4) and CT littermate (*Dyt1 loxP* +/−: n=1; *Dyt1 loxP* −/−: n = 3) male mice at 137–166 days-old were sacrificed and perfused with ice-cold 0.1M phosphate buffer (PB; pH 7.4) followed with 4% paraformaldehyde in 0.1M PB (pH 7.4). The brains were incubated with the fixative for overnight and then with 30% sucrose in 0.1M PB for another overnight until the brain sank. Each brain was frozen with dry-ice powder and coronal sections with 40 μm thickness were prepared by using a sliding microtome. The brain slices corresponding to the striatum were incubated with the primary and secondary antibodies as listed in Appendix Table A.1.

The slices were washed three times in 10 mM glycine/0.1M PB for 5 min each and blocked in 2% gelatin/0.1M PB for 15 min, 10 mM glycine/0.1M PB for 5 min and 0.1% BSA/0.1M PB for 5 min. The blocked slices were incubated in goat anti-ChAT antibody (EMD Millipore, AB144P; 1:50 dilution) or a combination of the anti-ChAT antibody and rabbit anti- cleaved caspase 3 (CC3) antibody (Cell signaling, #9664L: 1:50 dilution) in 1% bovine serum albumin (BSA)/0.1M PB at room temperature for 2 hours and 4 °C overnight. The slices were washed in 0.1% BSA/0.1M PB for six times at 5 min each. The slices were then incubated with Alexa Fluor 488 donkey anti-goat IgG (H+L) (Invitrogen, A11055; 1:200 dilution), or a combination of the Alexa Fluor 488 donkey anti-goat IgG and Alexa Fluor 546 donkey anti-rabbit IgG, in 1% BSA/0.1M PB for 2 hours and then washed in 0.1% BSA/0.1M PB for 5 min each six times. The slices were mounted on glass slides with Vectashield Hard Set mounting medium for fluorescence (Vector Lab Inc., H-1400) stored at 4°C overnight. The single- or double-positive cells were confirmed by using ZEISS Axiophot RZGF-1 microscope with Plan-NEOFLUAR objective lens, and FITC filter for Alexa Fluor 488 and Texas Red filter for Alexa Fluor 594, and digitized by using MBF Bioscience Neurolucida 7 and NeuroExplorer software (MicroBrightFields Bioscience). The density of immuno-positive neurons was calculated as the number of positive neurons per striatal area size (Yokoi et al., 2009). Representative images of the striatal ChAT-positive cells were taken by using Keyence All-in-one Fluorescence Microscope BZ-X810.

The brain slices corresponding to the substantia nigra were blocked and washed as described above and incubated in a mouse anti-TH antibody (Santa Cruz; sc-374047), or a

Author Manuscript Author Manuscript Author Manuscript Author Manuscript

combination of goat anti-TH and rabbit anti-CC 3 antibodies. The brain slices were then washed in 0.1% BSA/PB and incubated with the secondary antibodies conjugated with different fluorescence for 2 hours as appropriate, *i.e.*, Alexa Fluor 488 donkey anti-mouse IgG and the Alexa Fluor 546 donkey anti-rabbit IgG. The density of immuno-positive neurons was calculated as the number of the TH-positive somas per the area size of substantia nigra compacta (SNc) or substantia nigra reticulata (SNr). Representative images of the TH-positive cells were taken by using Nikon Confocal Microscope A1R HD25.

2.4. Electrophysiological recording of striatal MSNs in the indirect pathway

Acute brain slices were prepared from 5 CT and 3 d2KO male littermates at an average age of 4 months for the electrophysiological recording of striatal MSNs. Animals were sacrificed, and the brains were rapidly removed. 300 μm-thick coronal brain slices containing the dorsal striatum were cut in ice-cold, oxygenated cutting saline (in mM): 180 sucrose, 2.5 KCl, 1.25 NaH_2PO_4, 25 $NaHCO_3$, 10 D-glucose, 1 $CaCl_2$, 10 $MgCl_2$, and 10 glucose with a Vibratome (Leica VT 1000s). Slices were recovered in a holding chamber for 60 minutes at 35°C with artificial cerebrospinal fluid (ACSF; in mM: 126 NaCl, 2.5 KCl, 1.25 NaH_2PO_4, 25 $NaHCO_3$, 2 $MgCl_2$, 2 $CaCl_2$, and 10 glucose, pH = 7.3 with KOH, osmolality = 290–300 mOsm) with an application of 50 μM picrotoxin (PTX; Sigma) solution. The slices were then incubated at room temperature. The slices were placed in a recording chamber and continuously perfused with ACSF that was bubbled via 5% CO_2 and 95% O_2 at a rate of 1.5 ml/min while being visualized with an upright microscope (Zeiss, Germany) using a 40× water-immersion objective with infrared optics. MSNs were identified by the somatic size, basic membrane properties and characteristic evoked action potentials, *i.e.*, a prominent slowly depolarizing (ramp) potential and long latency to spike discharge (Nisenbaum et al., 1994). The microelectrode with the internal solution containing 0.1% biocytin was used to identify the recorded MSN. All experiments were recorded at 32°C by a dual automatic temperature controller (TC-344B). Recording patch pipette (6–10 MΩ) contained following solutions (in mM): 125 K-gluconate, 8 NaCl, 10 HEPES, 2 MgATP, 0.3 NaGTP, 0.2 EGTA, 0.1% biocytin (pH 7.25–7.3, osmolality, 290–300 mOsm) was used for both current and voltage-clamp recordings.

The intrinsic membrane properties of MSNs were determined in current-clamp mode by applying a depolarizing step current command (50 pA), Action potentials were evoked by step-current injections in whole-cell current-clamp, injection of depolarizing 50 pA current pulse of 300 ms duration evoked spike firing when the membrane potential reaches the firing threshold under current-clamp configuration in a brain slice. This process was repeated at 10 increasingly depolarized potentials with incremental current steps (50pA). MSNs were also identified by somatic size, basic membrane properties (membrane capacitance and membrane resistance). At holding potential –70 mV, spontaneous excitatory postsynaptic currents (sEPSCs) were further recorded by whole-cell voltage-clamp to analyze pre-synaptic and post-synaptic properties. Recordings were made from targeted striatal cells in the presence of PTX (50μM) using infrared differential interference contrast microscopy and an Axopatch 1D amplifier (Axon Instruments, Foster City, CA). Data were acquired using pClamp 10 software. Signals were filtered at 5 kHz, digitized at 10 kHz with a DigiData 1440 (Molecular Devices, Union City, CA). Membrane potentials were corrected with a

Author Manuscript Author Manuscript Author Manuscript Author Manuscript

calculated liquid junction potential of 15.7 mV. Events were detected using the Mini Analysis Program (Synaptosoft) with parameters optimized for each cell and then visually confirmed prior to analysis. The peak amplitude, 10–90% rise time and the decay time constant were measured based on the average of all events aligned by the rising phase. The electrophysiological recording was performed by an investigator blind to the genotypes.

2.5. Histochemical identification of the recorded striatal MSNs in the indirect pathway

Since the neurons were recorded with the internal solution containing 0.1% biocytin, the recorded neurons were identified by staining with Alexa Fluor 594-conjugated streptavidin through biocytin-streptavidin binding. After the electrophysiological recording, the brain slices were subsequently fixed overnight with 4% paraformaldehyde in 0.1M PB. Antigen retrieval (50 mM sodium citrate, 30 min, 80 °C) was performed, and the slices were rinsed with 0.5% Triton X-100 and 0.1% Triton X-100 in 0.02M PB for 5 min each. The slices were washed three times in 10 mM glycine/0.1M PB for 5 min each and blocked in 2% gelatin/0.1M PB for 15 min, 10 mM glycine/0.1M PB for 5 min and 0.1% BSA/0.1M PB for 5 min. The blocked slices were incubated with a combination of the goat anti-adenosine A_{2A} receptor (A2A) antibody (Santa Cruz, sc- 7504; 1:50 dilution) and streptavidin Alexa Fluor 594 conjugate (Life technologies, S11227; 1:500 dilution) in 1% BSA/0.1M PB at 4 °C overnight. Then the sections were washed in 0.1% BSA/0.1M PB for six times at 5 min each. The slices were then incubated with Alexa Fluor 488 donkey anti-goat IgG (H+L) (Invitrogen, A11055; 1:200 dilution) in 1% BSA/0.1M PB for 2 hours and then washed in 0.1% BSA/0.1M PB for six times at 5 min each. The slices were mounted on glass slides with Vectashield Hard Set mounting medium for fluorescence (Vector Lab Inc., H-1400) and covered with cover glass, and then stored at 4°C overnight. The double-positive cells were confirmed by using ZEISS Axiophot RZGF-1 microscope with FITC filter for Alexa Fluor 488 and Texas Red filter for Alexa Fluor 594, respectively. The representative images were taken by using 40× Plan-NEOFLUAR objective lens. Only the recording data from the double-stained neurons (CT: 11 neurons; d2KO: 18 neurons) were used for statistical analysis.

2.6. Motor behavioral tests

Motor performance of the *Dyt1* d2KO (male: n = 10, female: n = 10) and CT littermate mice [male: n = 10 (*Dyt1 loxP* +/−: n=1; *Dyt1 loxP* −/−: n=7; *D2-cre* +/−: n=1; WT: n=1); female: n = 13 (*Dyt1 loxP* +/−: n=5; *Dyt1 loxP* −/−: n=8)] was evaluated by general observation of dystonic movements, open-field, accelerated-rotarod, beam-walking, and paw-print gait analysis tests in this order. Briefly, the behavioral semi-quantitative assessments of motor disorders were performed as previously described (Dang et al., 2005; Fernagut et al., 2002). Each mouse at 157–221 days-old was placed on the table and assessments of hind paw clasping, hind paw dystonia, truncal dystonia and balance adjustments to a postural challenge were made. The hind paw clasping was assessed as hind paw movements for postural adjustment and attempt to straighten up while the mouse was suspended by the mid-tail.

An open-field test was performed during the light period as previously described (Cao and Li, 2002) with a minor modification. In brief, spontaneous locomotor activities of the mice

Author Manuscript Author Manuscript Author Manuscript Author Manuscript

at 161–224 days-old were recorded individually by infrared light beam sensors in a 41 × 41 × 31 cm acryl case directly illuminated by a 60 W white bulb for 30 min at 1 min intervals using DigiPro software (AccuScan Instruments).

The accelerated rotarod test assesses the ability of mice to maintain balance and coordination on an acceleratingly rotating rod. The motor performance of the mice at 164–228 days-old was examined with an accelerating rotarod (Ugo Basile) as previously described (Dang et al., 2005) with minor modification. The apparatus started at an initial speed of 4 rpm, and then each mouse was put on the same slot one by one. The rod speed was gradually accelerated at a rate of 0.2 rpm/s. The latency to fall was measured with a cutoff time of 5 min at a final rate of 64 rpm. Mice were tested for three trials on each day for 2 days. The trials within the same day were performed at about 1 h intervals.

The beam-walking test was performed as described earlier (Dang et al., 2005; DeAndrade et al., 2011; Yokoi et al., 2006; Yokoi et al., 2012c) and modified from others (Carter et al., 2001). The mice at 174–238 days-old were trained to transverse a medium square beam (14 mm wide) in three consecutive trials each day for 2 days. The trained mice were tested twice on the medium square beam and medium round beam (17 mm diameter) on the third day, and small round beam (10 mm diameter) and small square beam (7 mm wide) on the fourth day. The hind paw slips on each side were recorded.

The paw-print test is an analysis of the animal's gait. A runway with a dark goal box at the end was lined with a sheet of white paper (Carter et al., 2001). Fore and hind paws of the mice at 198–262 days-old were painted with water-soluble, non-toxic paint of different colors. Mice walked across the runway and into the goal box. One set of prints was collected for each animal after it walked continuously across the runway. The four center pairs of hind and forepaw prints of each set were analyzed for stride length, fore and hind base lengths, and distance of overlap of the paws.

2.7. Monoamine content analysis

After the motor behavioral tests, the same set of mice at 204–269 days-old were used for analyzing striatal monoamine contents. The striatal tissues were dissected and quickly frozen in liquid nitrogen. The monoamine contents were measured by using an analytical HPLC in the Neurochemistry Core Lab at the Vanderbilt University (VU) Medical center, Nashville TN.

2.8. Statistics

The ratio of genotypes was analyzed with Fisher's exact test. The Western blot signals were analyzed by using a linear mixed-effects model (lme) in R version 3.5.3 with duplications as the repeated measurement and a random effect. Densities of the immuno-positive cells (cell/mm^2) in FIHC, were analyzed by a mixed procedure with repeated measure in SAS/STAT software. Electrophysiological recording data were analyzed by SAS/STAT mixed procedures for normally distributed data or GENMOD procedure with log link for gamma distribution when they were not normally distributed. Open-field test and paw-print test data were analyzed by the mixed procedure in SAS/STAT software. Shapiro test was used to analyze the distribution of data with R. The data of latency to fall in accelerated rotarod test

Author Manuscript Author Manuscript Author Manuscript Author Manuscript

were analyzed by R linear mixed model with hierarchically concerning genotype, sex, weight, and age by Akaike Information Criterion (AIC). The slip numbers in the beam-walking test for all four beams were analyzed together by R generalized linear mixed model with negative binomial distribution and hierarchically concerning genotype, sex, weight, and age by AIC. The striatal neurochemicals were analyzed by Welch's t-test. Pearson correlations among the striatal neurochemicals and spontaneous locomotor activities were analyzed by R cor() and corr.test() programs. Significance was assigned at $p < 0.05$.

3. Results

3.1. Generation of the Dyt1 d2KO mice

Dyt1 d2KO mice were generated to examine the *in vivo* function of torsinA in the D2R-expressing cells. *Drd2-Cre* +/− *Dyt1 loxP* +/− (double heterozygote: DHet) were generated by crossing *Drd2-Cre* mice (Gong et al., 2007) and *Dyt1 loxP* mice (Yokoi et al., 2008). *Dyt1* d2KO mice were generated by crossing the DHet mice and either *Dyt1 loxP* +/− or *Dyt1 loxP* −/− mice, *i.e.*, DHet mice were crossed with *Dyt1 loxP* +/− mice to generate *Drd2-Cre* +/− *Dyt1 loxP* −/− (d2KO), *Drd2-Cre* +/− *Dyt1 loxP* +/− (DHet), *Drd2-Cre* +/− (*Cre* +/−), *Dyt1 loxP* −/−, *Dyt1 loxP* +/−, and *Dyt1 loxP* +/+ (WT) mice (Fig. 1A). DHet mice were also crossed with *Dyt1 loxP* −/− mice to generate *Drd2-Cre* +/− *Dyt1 loxP* −/− (d2KO), *Drd2-Cre* +/− *Dyt1 loxP* +/− (DHet), *Dyt1 loxP* −/−, and *Dyt1 loxP* +/− mice (Fig. 1B). Genotyping was performed by using PCR with tail DNA (Appendix Fig. A.1). The ratio of the obtained *Dyt1* d2KO mice did not deviate from Mendel's rule (Appendix Table B.1), suggesting that *Dyt1* d2KO mice are neither embryonic nor neonatal lethal. *Dyt1* d2KO mice grew up to adulthood without obvious developmental delay. The striatum contains mainly four types of D2R-expressing neurons, *i.e.* indirect pathway MSNs, ChIs, the axons of dopaminergic neurons projected from the substantia nigra compacta, and axons of the corticostriatal neurons (Gaspar et al., 1995). The population of the indirect pathway MSNs is about 45% and that of ChIs is only 1–2% in the striatal neurons. Since *Drd2-cre* was supposed to express in these neurons and delete the floxed *Dyt1* in the *Dyt1* d2KO mice, the torsinA level in the striatal tissue was measured by Western blot to examine the effect of the conditional KO. The data were analyzed by a linear mixed-effects model. The coefficients of each genotype that affect the detected protein ratio are shown in Appendix Table C.1, which summarizes all analyzed Western blot results in this study. The striatal torsinA level was significantly reduced in *Dyt1* d2KO mice [torsinA (~35.4 kDa)/GAPDH (~34.6 kDa); control (CT; n=6): 100 ± 4.9 %; *Dyt1* d2KO (n=8): 67.7 ± 4.6 %; $p = 0.0016$; Fig. 2A]. Since striatal D2R-non- expressing cells, such as the direct pathway MSNs, which account for ~45% of striatal neurons, glia cells, blood vessel cells and other cells, are supposed to express torsinA in *Dyt1* d2KO mice, the observed reduction level of striatal torsinA suggests a successful high deletion yield of *Dyt1* in the D2R-expressing cells.

3.2. Reductions of striatal D2R dimers and tyrosine hydroxylase in Dyt1 d2KO mice

The striatal D2R levels were analyzed by Western blot analysis. *Dyt1* d2KO mice showed a significant reduction of the D2R double-bands migrated at ~105 and 96.1 KDa [D2Rs/β-tubulin (~53.5 kDa); CT (n=6): 100 ± 13.2 %; *Dyt1* d2KO (n=8): 68.3 ± 4.6 %; $p = 0.026$; Fig. 2B]. Moreover, *Dyt1* d2KO mice showed a trend of reduction of the D2R band migrated

Author Manuscript Author Manuscript Author Manuscript Author Manuscript

at ~59.1 kDa [D2R/β-tubulin; CT (n=6): 100 ± 7.8 %; *Dyt1* d2KO (n=8): 82.5 ± 4.9 %; p = 0.077; Fig. 2B]. The striatal D2Rs migrated at ~105 and 96.1 KDa correspond to the manure form of D2R dimers, whereas the D2Rs migrated at ~59.1 KDa correspond to D2R monomers (Ng et al., 1996; Zawarynski et al., 1998). The results suggest that a loss of torsinA in the D2- expressing cells causes the reductions of D2Rs, especially the mature form of D2R dimers.

On the other hand, there was no significant difference in either the DARPP-32 [DARPP- 32 (~30.4 kDa)/β-tubulin; CT (n=6): 100 ± 5.2 %; *Dyt1* d2KO (n=8): 83.8 ± 6.3 %; p = 0.213; Fig. 2C;] or the phosphorylated DARPP-32 levels [p-DARPP-32 (~30.4 kDa)/β-tubulin; CT (n=6): 100 ± 10.1 %; *Dyt1* d2KO (n=8): 92.0 ± 8.2 %; p = 0.570; Fig. 2D]. DARPP-32 antibody binds all DARPP-32, whereas the phosphorylated DARPP-32 antibody binds only phosphorylated DARPP-32. Although DARPP-32 is expressed in both D1 and D2-expressing MSNs, the signal transduction pathways to phosphorylate DARPP-32 have opposite direction between these neurons, *i.e.*, DA binding on D1R stimulates phosphorylation of DARPP-32 and that on D2R inhibits phosphorylation of DARPP-32 (Avanes et al., 2019; Beaulieu and Gainetdinov, 2011). Since there was no significant difference in the striatal phosphorylated DARPP-32 levels between *Dyt1* d2KO mice and CT mice, the overall status of the striatal DARPP-32 pathway seems not to be affected by the loss of torsinA function in D2-expressing cells.

The striatal TH levels were further measured by Western blot to examine the effect of the conditional KO in the dopaminergic neurons. *Dyt1* d2KO mice showed a significant reduction of the striatal TH levels [TH (~61.2 kDa)/β-tubulin; CT (n=6), 100 ± 5.3 %; *Dyt1* d2KO (n=8), 82.4 ± 3.8 %; p = 0.017; Fig. 2E], suggesting a malfunction of dopamine synthesis.

The striatum contains many axons of the striatal dopaminergic neurons projected from the SNc. The coronal brain slices were stained with TH antibody to examine whether the reduced striatal TH was caused by a loss of dopaminergic neurons or not (Fig. 3A, B). The area sizes of SNc were measured and the numbers of the TH-positive somas were counted in SNc. There was no significant difference in the density of TH-positive neurons in SNc between CT and *Dyt*1 d2KO mice [the number of TH-positive somas per the unit area size; positive somas ± standard errors somas/mm^2; SNc, CT (n=4): 508 ± 42; d2KO (n=4): 571 ± 99; p = 0.58; Fig. 3C]. Therefore, the reduced striatal TH level may be caused by a low expression of TH rather than a reduced number of dopaminergic neurons. The results suggest that the conditional KO did not affect the number of dopaminergic neurons in SNc. The area sizes of SNr were also measured and the numbers of the TH-positive somas in SNr were counted to compare the density of dopaminergic neurons between the SNc and SNr. There was no significant difference in the density of TH-positive neurons in SNr between CT and *Dyt*1 d2KO mice (somas/mm^2; CT: 144 ± 29; d2KO: 173 ± 28; p = 0.49; Fig. 3D). The results suggest that the conditional KO did not affect the number of dopaminergic neurons in both SNc and SNr.

Author Manuscript Author Manuscript Author Manuscript Author Manuscript

3.3. Reductions of the striatal cholinergic interneurons in Dyt1 d2KO mice

Acetylcholine (ACh) metabolic enzyme levels in the striatal tissues were measured by Western blot to examine the effect of torsinA loss on the striatal cholinergic system. *Dyt1* d2KO mice showed significant reductions of ChAT [ChAT (~67.5 kDa)/β-tubulin; CT (n=6): 100 ± 4.3 %; *Dyt1* d2KO (n=8): 86.3 ± 4.3 %; $p = 0.029$; Fig. 4A] and VAChT [VAChT (~68.2 kDa)/β- tubulin; CT (n=6): 100 ± 10.5 %; *Dyt1* d2KO (n=8): 57.2 ± 4.6 %; $p = 0.0015$; Fig. 4B]. Moreover, *Dyt1* d2KO mice showed a trend of reduction of the ChT bands migrated at ~71.5 kDa [ChT/β- tubulin; CT (n=6): 100 ± 3.7 %; *Dyt1* d2KO (n=8): 84.1 ± 5.9 %; $p = 0.058$; Fig. 4C] and ~58.9 kDa [ChT/β-tubulin; CT (n=6): 100 ± 6.0 %; *Dyt1* d2KO (n=8): 81.2 ± 7.5 %; $p = 0.089$; Fig. 4C]. The ChT migrated at ~71.5 kDa corresponds to a glycosylated manure form, whereas that migrated at ~58.9 kDa corresponds to a premature form (Bergeron et al., 2005; Berse et al., 2005). The results suggest a malfunction of the striatal ACh production in the *Dyt1* d2KO mice. On the other hand, the *Dyt1* d2KO mice showed a normal level of the striatal AChE [AChE (~67.4 kDa)/GAPDH; CT (n=6): 100 ± 4.6 %; *Dyt1* d2KO (n=8): 108.2 ± 6.9 %; $p = 0.37$; Fig. 4D]. The results suggest that the degradation of ACh is normal in *Dyt1* d2KO mice. Since the striatal ChIs highly express TrkA, it is often used as one of the ChI markers. Consistent with the reduced ChAT and VAChT, *Dyt1* d2KO mice showed a significant reduction of TrkA [TrkA (~133.6 kDa)/β-tubulin; CT (n=6): 100 ± 3.5 %; *Dyt1* d2KO (n=8): 70.5 ± 5.0 %; $p = 0.0007$; Fig. 4E].

The densities of the striatal ChIs were analyzed by measuring the area size of the striatum and counting the striatal ChAT-positive neurons in FIHC to examine whether the reduced ChI marker enzymes were caused by a reduction of ChI number or not (CT: Fig. 5A and C; *Dyt1* d2KO: Fig. 5B and D). *Dyt1* d2KO mice showed a significant reduction of the ChAT-positive neuron density [CT (n=4): 27.2 ± 3.6 ChIs/mm^2; *Dyt1* d2KO (n=4): 14.7 ± 3.6 ChIs/mm^2; $p = 0.0286$; Fig. 5I], suggesting that the reductions of the ACh metabolic enzymes, *i.e.* ChAT, VAChT and ChT, detected in the Western blot analysis were caused by the reduced number of ChIs. The CC3 is an indicator of the apoptotic cell. The densities of the striatal ChAT and CC3 double-positive neurons were further analyzed by measuring the area size of the striatum in another set of brain slices and counting the striatal ChAT and CC3 double-positive neurons in FIHC to examine whether the reduction of the ChIs in *Dyt1* d2KO mice was caused by on-going apoptosis or not [CT: ChAT (Fig. 5E), *Dyt1* d2KO: ChAT: (Fig. 5F), CT: CC3 (Fig. 5G), *Dyt1* d2KO: CC3 (Fig. 5H)]. The ChAT and CC3 double-positive neurons were very rare in both CT and *Dyt1* d2KO mice. There was no significant difference in the density of CC3-positive ChIs [CT (n=4): 0.042 ± 0.016 ChIs/mm^2; *Dyt1* d2KO (n=4): 0.053 ± 0.023 ChIs/mm^2; $p = 0.71$; Fig. 5J], suggesting that the reduction of striatal ChI occurred much earlier.

3.4. The increased membrane resistance of the striatal indirect pathway MSNs in d2KO mice

More than 90% of the striatal neurons are MSNs and half of them are D2-expressing MSNs which contribute to the indirect pathway in the basal ganglia circuits, whereas another half are D1-expressing MSNs which contribute to the direct pathway. To examine the effect of torsinA loss in the indirect pathway MSNs, we characterized their electrophysiological properties in whole cell recording mode. After recording, the brain slices were stained with

Author Manuscript Author Manuscript Author Manuscript Author Manuscript

Alexa Fluor 594-conjugated streptavidin through biocytin-streptavidin binding to identify the recorded neurons (Fig. 6A) and further stained with anti-A2A primary and Alexa Fluor 488-conjugated secondary antibodies to identify the striatal indirect pathway MSNs (Fig. 6B). A2A was stained at the cellular membrane of the indirect pathway MSNs as previously reported (Rosin et al., 1998; Trusel et al., 2015). Only the electrophysical recording data of the double-stained neurons were used for statistical analysis described below.

The intrinsic electrophysiological membrane properties of the striatal indirect pathway MSNs were measured in the whole cell recording (Table 1). The d2KO mice showed a significantly increased membrane resistance comparing to those in CT littermate mice (Rm: coefficient: CT: −0.1795 ±0.0877; d2KO: 0; p=0.0408). On the other hand, there was no significant difference between CT and d2KO mice in the resting membrane potential (RMP), the membrane capacitance, or the time constant.

Action potentials were evoked by step-current injections in whole cell current-clamp (CT: Fig. 6C; d2KO: Fig. 6D). The recording trances showed a typical characteristic of the striatal MSNs, *i.e.*, a prominent slowly depolarizing (ramp) potential and long latency to spike discharge in response to intracellular current pulses (Nisenbaum et al., 1994). A total of 24 striatal indirect pathway MSNs (CT: 16 cells/n=5 mice; d2KO: 8 cells/n=3 mice) were recorded. SAS GENMOD procedure was used to analyze the number of action potentials evoked by each step-current injection with gamma distribution with log link. There was no significant difference between CT and d2KO mice in the number of evoked action potentials (coefficient of genotype; CT: 0; d2KO: –0.067 ± 0.087; p=0.51; Fig. 6E). Moreover, there was no significant alteration in other kinetics parameters of the evoked action potentials between CT and d2KO mice (Table 2).

Spontaneous sEPSCs were further recorded by whole-cell voltage-clamp to analyze pre-synaptic and post-synaptic properties (CT: 16 cells/n=5 mice; d2KO: 8cells/n=3 mice; Fig. 6F). The frequency was analyzed by the GENMOD procedure with a log link and gamma distribution. There was no significant difference in the frequency of sEPSCs between CT and d2KO mice (coefficient of genotype; CT:0, d2KO: −0.2568 ± 0.3363, p=0.445; Fig. 6G). Moreover, there was no significant alteration in other kinetics parameters of the sEPSCs between CT and d2KO mice (Table 3). The results suggest that sEPSCs were normal in d2KO mice.

3.5. Motor deficits in Dyt1 d2KO mice

Since the striatal D2R-expressing neurons contribute to motor coordination, motor behaviors of *Dyt1* d2KO mice (male: n=10, female: n=10) were evaluated and compared to those in CT mice (male: n=10, female: n=13) by multiple motor behavior tests, *i.e.*, general observation of dystonic movements, open-field, accelerated-rotarod, beam-walking and paw-print tests in this order. Behavioral semi-quantitative assessments of motor disorders revealed that the *Dyt1* d2KO mice did not show overt dystonic symptoms. The spontaneous locomotion of *Dyt1* d2KO mice was further evaluated by the open-field test (Appendix Table D.1) and was found to be normal.

Author Manuscript Author Manuscript Author Manuscript Author Manuscript

The motor performance that requires all four paws was evaluated by an accelerated- rotarod test. Each mouse was put on an accelerated-rotarod and the latency to fall was measured. Shapiro test suggested that the accelerated rotarod test data of averaged latency to fall in the six trials showed normal distribution (p=0.9945). The data of latency to fall were analyzed by R linear mixed model with concerting body weight as lowest AIC. Coefficients of genotype to the latency to fall are shown in Appendix Table E.1–E.3. There was a trend of decreased latency to fall in d2KO mice but no significant difference in the averaged latency to fall between CT and d2KO mice (p=0.0829; Fig. 7A, Appendix Table E.1). The data were further analyzed in each trial. *Dyt1* d2KO mice showed a significant reduction of latency to fall at the second trial (p=0.0158; Appendix Table E.1). Since there was a significant interaction between genotype and sex (p=0.00163), the latency to fall data were stratified by sex and analyzed further. *Dyt1* d2KO male mice showed significantly decreased averaged latency to fall than CT male mice (p=0.0323; Fig. 7B, Appendix Table E.2), suggesting motor deficits in *Dyt1* d2KO male mice. Comparison in each trial showed that *Dyt1* d2KO male mice exhibited significantly decreased averaged latency to fall than CT male mice at the first and second trials and a trend of decreased latency to fall at 6th trial (p= 0.0144, 0.0097, and 0.0889, respectively; Appendix Table E.2). On the other hand, there was no significant difference in the averaged latency to fall between CT and *Dyt1* d2KO female mice (p=0.2343; Fig. 7C, Appendix Table E.3). Comparison in each trial showed that *Dyt1* d2KO female mice exhibited only a trend of decreased latency to fall at the second trial (p=0.0932; Appendix Table E.3). Overall, the accelerated rotarod test suggested that *Dyt1* d2KO male mice showed significant motor deficits, especially at the first and second trials. On the other hand, *Dyt1* d2KO female mice did not show significant motor deficits.

The motor performance of the hind-limbs was further evaluated with the beam-walking test. Since the Shapiro test suggested that the slip numbers were not normally distributed (p=3.857×10^{-9}), R generalized linear mixed model was used to analyze the slip numbers in the beam-walking test with negative binomial distribution concerning body weight and age. *Dyt1* d2KO mice showed a significant increase of slip number means in the beam-walking test (slip numbers; mean ± standard errors; CT: 4.8 ± 1.4; d2KO: 13.3 ± 3.8; p = 0.0161; Fig.7D, Appendix Table F.1), suggesting motor deficits in *Dyt1* d2KO mice. Since there was a significant interaction between genotype and sex (p=0.00109), the data were stratified by sex and the slip numbers were analyzed further in each sex. *Dyt1* d2KO male mice showed a significant increase of total slip numbers in the beam-walking test (CT: 4.3 ± 1.2; d2KO: 22.6 ± 6.3; p=0.0000589; Fig.7E, Appendix Table F.1), suggesting motor deficits of hind limbs in *Dyt1* d2KO male mice. On the other hand, there was no significant difference in total slip numbers between CT and *Dyt1* d2KO female mice, suggesting that no motor deficit of hind limbs was detected *Dyt1* d2KO female mice (CT: 5.2 ± 1.7; d2KO: 3.9 ± 1.7; p=0.4976; Fig.7E, Appendix Table F.1).

The gait performance was further analyzed by the paw-print test. The distances of the stride, fore and hind bases, and overlap were compared between *Dyt1* d2KO (n=20) and CT mice (n=23; Fig. 7F). *Dyt1* d2KO mice did not show any significant gait alterations, *i.e.*, in the stride [mean ± standard errors (mm): CT: 70.2 ± 1.3; *Dyt1* d2KO: 68.5 ± 1.4; p = 0.39], forelimb base (CT: 14.5 ± 0.5; *Dyt1* d2KO: 15.2 ± 0.6; p = 0.39), hind limb base (CT: 26.8 ±

Author Manuscript Author Manuscript Author Manuscript Author Manuscript

0.8; *Dyt1* d2KO: 27.3 ± 0.8; $p = 0.69$), and overlap (CT: 9.3 ± 0.7; *Dyt1* d2KO: 8.8 ± 0.8; $p = 0.62$).

3.6. Striatal dopamine, serotonin and their metabolite levels in Dyt1 d2KO mice

The striatal tissue monoamine contents of the behavioral test batch were measured by the analytical high performance of liquid chromatography to examine whether the reduced striatal TH level in the *Dyt1* d2KO mice affects the tissue dopamine level or not (HPLC; Table 4). There was no significant alteration in dopamine and its metabolites between the *Dyt1* d2KO and CT mice. The data were stratified by sex and analyzed further (Table 5). Although most of the monoamine contents and their turnover were normal in each sex, there was a significant increase of 5-hydroxyindoleacetic acid (5-HIAA)/serotonin (5-hydroxytryptamine; 5-HT) ratio in the *Dyt1* d2KO male mice. On the other hand, the *Dyt1* d2KO female mice showed a significant increase of 3-MT. The *Dyt1* d2KO female mice also showed a significantly decreased DOPAC/DA ratio and a trend of decreased HVA/DA ratio. The results suggest that the striatal neurochemicals were mostly normal in the *Dyt1* d2KO mice except for a few sex-dependent changes.

3.7. Correlations between the striatal monoamines and spontaneous motor behaviors in Dyt1 d2KO mice

Correlations between the striatal monoamine contents and locomotor activity in the open-field test were analyzed (Table 6). The CT mice showed mostly no correlation between the striatal monoamine contents and locomotor, except for a significant negative correlation in HIAA and vertical movement time (VTIME). On the other hand, *Dyt1* d2KO mice showed significant negative correlations between Noradrenaline and stereotypic components, *i.e.*, stereotypic count (STRCNT) and time (STRTIME). *Dyt1* d2KO mice showed significant negative correlations between DOPAC/DA ratio and many locomotor components and positive correlation between DOPAC/DA and other components, *i.e.*, rest time (RESTIME) and marginal time (MRGTIME). *Dyt1* d2KO mice showed significant negative correlations between HVA/DA ratio and other horizontal locomotors, *i.e.*, horizontal activity (HACTV), total distance (TOTDIST), anticlockwise revolution (ACWREV), and central distance (CTRDIST). *Dyt1* d2KO mice showed significant positive correlations between DA and HACTV, and between DA and CTRDIST.

Correlations between the striatal monoamine contents and spontaneous motor behaviors were further analyzed in each sex separately. The correlations showing a significant difference ($p<0.05$) and their counterparts are listed in Appendix Table G.1. and those showing very significant difference ($p<0.01$) are summarized in Table 7. Noradrenaline negatively correlated with stereotypic movements, shown as STRCNT, stereotypic movement number (STRNO), and STRTIME, in *Dyt1* d2KO male mice. DPAC/DA ratio negatively correlated with HACTV, vertical movement number (VMOVNO), STRCNT, and STRNO in *Dyt1* d2KO male mice. 5-HIAA negatively correlated with central time (CTRTIME) in *Dyt1* d2KO male mice. Consistent with DPAC/DA ratio, HVA/DA also negatively correlated with HACTV, VMOVNO, and STRCNT in *Dyt1* d2KO male mice. 3-MT positively correlated with HACTV and STRCNT in *Dyt1* d2KO male mice. On the other hand, DOPAC/DA ratio positively correlated with STRNO in CT male mice. Moreover, 3-

Author Manuscript Author Manuscript Author Manuscript Author Manuscript

MT and 3-MT/DA ratio positively correlated with clockwise revolution (CWREV) in CT male mice. On the other hand, 5-HT negatively correlated with ACWREV in CT female mice. Overall, abnormal correlations between the locomotor activities and striatal monoamine contents were mainly observed in *Dyt1* d2KO male mice, but not in *Dyt1* d2KO female mice.

4. Discussion

Dyt1 d2KO mice were generated and characterized to examine the *in vivo* effects of torsinA loss in the D2R-expressing cells. *Dyt1* d2KO mice showed significant reductions of striatal torsinA, ChAT, VAChT and TrkA. Consistent with the reductions of the cholinergic neuron marker proteins, the number of striatal ChIs was reduced in *Dyt1* d2KO mice. Moreover, *Dyt1* d2KO mice showed significant reductions of the striatal D2R dimers and TH without significant change in the number of dopaminergic neurons in the SNc, which extend their axons into the striatum. Furthermore, *Dyt1* d2KO male mice showed motor deficits in the rotarod and beam-walking tests without overt dystonic symptoms. The results suggest that torsinA in the D2R-expressing cells play a critical role for the motor coordination and balance, and the development, survival, or both, of the striatal ChIs. The present results suggest the selective vulnerability of the striatal neurons in the basal ganglia circuits due to the loss of torsinA function.

The mechanism of the striatal ChIs reductions in *Dyt1* d2KO mice is not known. One of the possibilities is that loss of torsinA function in the ChIs may change maturation or expression of TrkA and affect the development or survival of ChIs. Since only ChIs express TrkA among all D2R-expressing striatal neurons, striatal ChIs may be selectively affected by the reduction of TrkA function, resulting in the reduction of NGF binding. There are many studies reporting the importance of TrkA as an NGF receptor for surviving of the cell lines and neurons in the central nervous systems (Fagan et al., 1997; Patel et al., 2000; Sanchez-Ortiz et al., 2012; Zhang et al., 2000). The striatal ChIs express TrkA and loss of striatal ChIs affects basal ganglia circuits. The striatal ChIs release ACh, which in turn affects the neuronal activities of the striatal MSNs, which express muscarinic acetylcholine receptors (AChRs) (Surmeier et al., 2007). Pausing of the ChI activities sends signals to the MSNs (Zucca et al., 2018). Moreover, ACh stimulates nicotinic acetylcholine receptors on the axons of the striatal dopaminergic neurons and induces DA release (Threlfell et al., 2012). The malfunction of ACh system in *Dyt1* d2KO mice may affect the neuronal activities of both striatal MSNs and dopaminergic neurons and contributes to the exhibition of motor deficits.

Dyt1 d2KO mice showed decreased striatal ChI numbers. Decreased striatal ChIs have been reported in two other torsinA conditional KO mouse models, *i.e.*, Dlx-CKO mouse, which is a forebrain-specific loss of torsinA mouse model (Pappas et al., 2015), and ChAT-CKO mice, which is a “cholinergic neuron-specific” loss of torsinA mouse model (Pappas et al., 2018). The forebrain-specific Dlx-CKO mouse has a heterozygous *Tor1a*/*Dyt1* knockout (KO) in one allele and *Dlx5/6-Cre*-mediated conditional KO in the other and exhibits a selective loss of both dorsolateral and dorsomedial striatal cholinergic interneurons and overt “dystonic” symptoms. The so-called “cholinergic neuron-specific” ChAT-CKO mouse has a

Author Manuscript Author Manuscript Author Manuscript Author Manuscript

heterozygous *Tor1a*/*Dyt1* knockout (KO) in one allele and *ChAT-cre*-mediated conditional KO in the other and exhibits a selective loss of both dorsolateral and dorsomedial striatal cholinergic interneurons and reduced latency to fall during forelimb suspension. Since both Dlx-CKO and ChAT-CKO were produced by combinations of heterozygous KO of torsinA and either Dlx- or ChAT-cre-mediated conditional KO in another allele, it wasn't clear whether the reduction of striatal ChIs is produced by the combination with heterozygous KO in the whole body or not. Here, *Dyt1* d2KO mice, which removed torsinA only in the D2R-expressing cells without heterozygous KO in the whole body, showed a reduction of striatal ChIs. The results suggest that the combination with heterozygous KO in the whole body is not essential for the loss of striatal ChIs.

In contrast to *Dyt1* d2KO, Dlx-CKO, and ChAT-CKO mice, ΔGAG KI (Song et al., 2013) and ChKO mice (Sciamanna et al., 2012) do not show a reduction of striatal ChIs. Furthermore, the ΔGAG KI mice show a 22% increase in ChIs density in the dorsolateral striatum. The ΔGAG KI mutation leads to a partial reduction of torsinA function. Different from ChAT-CKO mice, ChKO mice show only cholinergic neurons have torsinA loss. Therefore, the difference of the striatal ChIs reduction seems to be caused by magnitude and area of loss of torsinA function.

Here *Dyt1* d2KO mice showed a reduction of striatal ChIs. The *Dyt1* d2KO male mice also showed motor deficits in the accelerated rotarod and beam-walking tests. Increased slips in beam-walking are derived from hindlimb deficits. A recent study showed that targeted ~50% ablation of cholinergic interneurons in the dorsomedial striatum of mice led to a deficit in coordination on the rotarod (Xu et al., 2015). Moreover, interneuron ablation in the dorsolateral striatum led to stereotypies after either acute stress or D-amphetamine challenge. Motor deficits in the rotarod test are derived from both forelimb and hindlimb deficits. Therefore, the differences in motor deficits between the *Dyt1* d2KO mice and the interneuron-ablation mouse model may depend on different severity of the motor deficits and the extent of ChI loss. In conclusion, reduction of striatal ChIs caused by loss of torsinA function may contribute to motor deficits.

Despite the significant reduction of striatal ChIs, *Dyt1* d2KO male mice showed only motor deficits in the accelerated rotarod and beam-walking tests without overt dystonic symptoms. Consistent with the *Dyt1* d2KO male mice, many mutant mouse and rat models show motor deficits without overt dystonic symptoms as previously reviewed (Oleas et al., 2015; Oleas et al., 2013). These models contain a growing number of targeted and transgenic rodent models of DYT1 (Alvarez-Fischer et al., 2012; Dang et al., 2005; Dang et al., 2006; Page et al., 2010; Sciamanna et al., 2012; Song et al., 2012; Yokoi et al., 2015a; Yokoi et al., 2011; Yokoi et al., 2008; Zhao et al., 2008), DYT11 (Yokoi et al., 2006; Yokoi et al., 2005; Yokoi et al., 2012b; Yokoi et al., 2012c) and DYT12 (DeAndrade et al., 2011; Moseley et al., 2007). Contrasting with most of the mutant mouse models, overt dystonic symptoms are reported in Dlx-CKO mice which show a significant reduction of striatal ChIs. The dystonic symptoms in Dlx-CKO mice, however, cannot be attributed to either heterozygous knockout of the torsinA in the whole body or significant reduction of striatal ChIs because ChAT-CKO mice, which have heterozygous KO of the torsinA in whole body and significant reduction of striatal ChIs, do not show any overt dystonia. It should be noted that in Dlx-CKO mice,

Author Manuscript Author Manuscript Author Manuscript Author Manuscript

torsinA is removed from most of the inhibitory neurons in cerebral cortex and could potentially lead to a hyperactive, even epileptic, cortical circuit. The striatum of Dlx-CKO mice exhibits significant increases in functional connectivity with cerebral cortex (DeSimone et al., 2017). The questions of whether Dlx-CKO mice show cortical hyperactivity and if it could account for the overt dystonia remain to be investigated.

The *Dyt1* d2KO mice showed significantly increased membrane resistance of the striatal indirect pathway MSNs comparing to those in the CT littermate mice. Since torsinA function was impaired in the striatal indirect pathway MSNs in *Dyt1* d2KO mice as suggested by the reduction of striatal torsinA, the increased membrane resistance may be caused by the cell-autonomous effect of reduced torsinA in the striatal indirect pathway MSNs. Membrane resistance is increased when the opening of ion channels on the cellular membrane is reduced. Although the mechanism of increased membrane resistance in *Dyt1* d2KO mice is not known, previously published reports may provide a clue. For example, a cultured cell model suggests that torsinA contributes to regulating cellular trafficking of the dopamine transporter, as well as other polytopic membrane-bound proteins, including G protein-coupled receptors, transporters, and ion channels (Torres et al., 2004). Reduced ion channels on the cellular membrane may cause less transport of ions across the cellular membrane and increase membrane resistance of the neuronal membrane. It is also consistent with the impaired LTD in KI mice.

Functional alterations of the dopaminergic systems, such as reduction of striatal D2R, have been shown in DYT1 dystonia patients and rodent models. Here *Dyt1* d2KO mice (n=8) showed a significant ~31.7% reduction of the mature form of striatal D2R dimers and a trend of ~17.5% reduction of striatal D2R monomers, compared with CT mice (n=6) in Western blot analysis. The reduction of striatal D2R has been reported in other lines of DYT1 dystonia mouse models. A previous study using human wild-type torsinA-expressing transgenic mice (hMT; n=17) shows ~30% reduction of striatal D2R, compared to human wild-type torsinA-expressing mice (hWT; n=8) and non-transgenic mice NT; n=25) in Western blot analysis (Napolitano et al., 2010). Another previous study using *Dyt1* ΔGAG KI mice (n=3) show ~39% reduction of striatal D2R, compared with WT mice (n=3) in Western blot analysis (Dang et al., 2012). A recent study using another line of ΔGAG KI mice (n=9) shows ~35% reduction of striatal D2R, compared with WT mice (n=7) in Western blot analysis (Bonsi et al., 2019). Although functional defect of torsinA seems to reduce 30~39% of striatal D2Rs, there is a slight difference in the magnitude of the reduction levels between the mouse models. The magnitude difference may be caused by the different neurons affected by the different genetic manipulations of torsinA. Genetic background and age may also slightly affect the anatomical phenotypes because a genetic mouse model with different genetic background and age shows a slight different behavioral phenotype (Tanabe et al., 2012).

Moreover, a reduction of TH was reported in a dtrosin null-mutation of *Drosophila melanogaster* model (Wakabayashi-Ito et al., 2011). The fly model also shows semi-lethality, locomotion defects, significant reduction of GTP cyclohydrolase and dopamine. In the fly, dtrosin is the only ortholog of torsinA and torsinB. Therefore, it is not clear whether the reduction of TH is caused by the loss of torsinA-like function alone or the loss of all torsin

Author Manuscript Author Manuscript Author Manuscript Author Manuscript

family members. The present result suggests that a loss of only torsinA in the D2R-expressing cells causes a significant reduction of striatal TH.

The present results suggest that the striatal neurochemicals were mostly normal in the *Dyt1* d2KO mice except for a few sex-dependent changes. There was a significant increase in 5-HIAA/5-HT ratio in the *Dyt1* d2KO male mice. This may be caused by the combination of the trends of increased means of 5-HIAA and decreased means of 5-HT. On the other hand, the *Dyt1* d2KO female showed alterations in DA metabolism. DA is metabolized to 3-MT by Catechol-*O* methyl transferase (COMT) and 3-MT is further metabolized to HVA by Monoamine oxidase (MAO) and aldehyde dehydrogenase (ALDH) (Qi et al., 2008). DA is also metabolized to DOPAL by MAO and SSAO (semicarbazide-sensitive amine oxidase), and DOPAL (3,4- dihydroxyphenylacetaldehyde) is metabolized to DOPAC by ALDH. DOPAC is further metabolized to HVA by COMT. Since *Dyt1* d2KO female mice showed a significant increase of 3-MT, the DA→3-MT pathway catalyzed by COMT seems to be enhanced with a combination of the trend of increased DA. On the other hand, *Dyt1* d2KO female mice showed a significantly decreased DOPAC/DA ratio, suggesting that the DA→DOPAL→DOPAC pathway catalyzed by MAO, SSAO and ALDH seems to be attenuated. *Dyt1* d2KO female also showed a trend of decreased HVA/DA ratio. HVA is produced indirectly from DA through both DA→DOPAL→DOPAC→HVA and DA→3-MT→HVA pathways. The attenuated DA→DOPAL→DOPAC pathway may contribute to the trend of decreased HVA/DA ratio. Moreover, the 3-MT→HVA pathway catalyzed by MAO and ALDH may also be attenuated to show the trend of decreased HVA/DA ratio because the upstream DA→3-MT pathway seems to be enhanced. Transcriptions of MAO genes are regulated by multiple hormones, such as androgen and glucocorticoid to upregulate MAOA transcription, and the interplay of estrogen receptors and estrogen-related receptors in the regulation of MAO B transcription in other cells (Shih et al., 2011). The sex hormones affecting the MAOs' expression may contribute to the different DA metabolisms between the sexes in *Dyt1* d2KO mice. Examining whether *Dyt1* d2KO female mice show an enhanced COMT, and attenuated MAO, SSAO and ALDH or not will be a future study to elucidate the mechanism of the DA metabolism alterations.

Correlation analysis between the striatal monoamines and spontaneous locomotor behaviors showed alterations in *Dyt1* d2KO mice, especially in *Dyt1* d2KO male mice. Here, a very significant negative correlation between DOPAC/DA ratio and ACWREV was shown in *Dyt1* d2KO mice. Correlation between dopaminergic system defect and rotation behaviors has been reported (Ungerstedt and Arbuthnott, 1970). For example, a rat model rotates toward the side with the weaker dopaminergic neurotransmission (Da Cunha et al., 2008). The negative correlation between DOPAC/DA ratio and ACWREV in *Dyt1* d2KO mice may be influenced by an unbalanced alteration of striatal dopamine metabolism. Correlations between the striatal monoamine contents and spontaneous motor behaviors were further analyzed in each sex separately. Spontaneous movements were abnormally correlated with striatal monoamine, especially dopamine and its metabolites, in *Dyt1* d2KO male mice. On the other hand, only 5-HT negatively correlated with ACWREV in female CT mice. Sex-dependent differences in dopamine metabolism were reported in both rodents and humans (Munro et al., 2006; Ngun et al., 2011). The sex differences in the correlations may be dependent on the sex differences of the vulnerability of dopaminergic system.

Author Manuscript Author Manuscript Author Manuscript Author Manuscript

Although the striatal monoamine contents and locomotor behaviors in the open-field test were mostly normal, correlation analysis between striatal monoamine contents and locomotor behaviors in the *Dyt1* d2KO mice showed significant and broad correlations. In other words, spontaneous movements seem to be correlated with the striatal monoamine metabolism in *Dyt1* d2KO mice. In contrast with *Dyt1* d2KO mice, the CT mice showed mostly no correlation between monoamine contents and spontaneous motor behaviors, similar to the WT mice as described earlier (Yokoi et al., 2006). Therefore, the locomotor behaviors in both WT mice and CT mice show no direct correlation with the levels of striatal monoamine and their metabolites. On the other hand, this relationship seems to be disrupted in *Dyt1* d2KO mice and another DYT11 myoclonus-dystonia mouse model (Yokoi et al., 2006). Interestingly, like *Dyt1* KI mice, corticostriatal LTD and ChI dysfunction have been reported in another DYT11 mouse model (Maltese et al., 2017). The changes in correlation between locomotor behavior and striatal monoamine metabolism may relate to the involuntary movement in dystonia. A previous report shows that the increase of striatal extracellular DA following administration of L-DOPDA in the DA-depleted rats is significantly greater than that observed in intact rats (Abercrombie et al., 1990). Moreover, behavioral activation is observed following the administration of L-DOPDA to DA-depleted rats whereas few behavioral effects of L-DOPA are observed in intact rats. Since dopaminergic and cholinergic pathways have cross-talks with each other, striatal monoamines may affect motor behaviors more in animals with defected dopaminergic and cholinergic pathways than normal animals. Whether the correlations in *Dyt1* d2KO mice are the results of the reduction of striatal ChIs, TH, or both, remains to be investigated.

5. Conclusions

The *Dyt1* d2KO mice showed significant reductions of striatal torsinA, acetylcholine metabolic enzymes, TrkA, and cholinergic interneurons. The *Dyt1* d2KO mice also showed significant reductions of striatal D2R dimers and TH without significant alteration in striatal monoamine contents or the number of dopaminergic neurons in the substantia nigra. The *Dyt1* d2KO male mice showed motor deficits in the accelerated rotarod and beam-walking tests but no overt dystonia, despite the selective loss of striatal cholinergic interneurons. Moreover, the *Dyt1* d2KO male mice showed a significant correlation between striatal monoamines and locomotion. The results suggest that torsinA in the D2R-expressing cells play a critical role in the development or survival of the striatal cholinergic interneurons, expression of striatal D2R mature form, and motor performance. Medical interventions to compensate for the loss of torsinA function in these neurons may affect the onset and symptoms of this disease.

Supplementary Material

Refer to Web version on PubMed Central for supplementary material.

Acknowledgements

We thank the animal colony staff for animal care. We also thank Jareisha Vickers, Aysha Awal, and other undergraduate students in UF and the staff in the VU for their technical assistance.

Author Manuscript Author Manuscript Author Manuscript Author Manuscript

Funding

This work was supported by Tyler's Hope for a Dystonia Cure, Inc., National Institutes of Health (NS37409, NS47466, NS47692, NS54246, NS57098, NS65273, NS72782, NS74423, NS75012, and NS82244), startup funds from the Lucille P. Markey Charitable Trust and Beckman Institute (UIUC), Department of Neurology (UAB), Dystonia Medical Research Foundation, and Bachmann-Strauss Dystonia and Parkinson Foundation, Inc. FY was partially supported by the Office of the Assistant Secretary of Defense for Health Affairs through the Peer-Reviewed Medical Research Program Discovery Award under Award No. W81XWH1810099. Opinions, interpretations, conclusions, and recommendations are those of the author and are not necessarily endorsed by the Department of Defense.

Abbreviations

ACh	acetylcholine
AChE	acetylcholinesterase
ACWREV	anticlockwise revolution
ACWREV	anticlockwise revolution
AIC	Akaike Information Criterion
ALDH	aldehyde dehydrogenase
BSA	bovine serum albumin
CC3	cleaved caspase 3
ChAT	choline acetyltransferase
ChI	cholinergic interneuron
ChT	choline transporter
COMT	Catechol-*O* methyl transferase
CT	control
CTRDIST	central distance
CTRTIME	central time
CWREV	clockwise revolution
DA	dopamine
DHet	double heterozygote
Dlx-CKO mice	Dlx-cre-derived forebrain-specific conditional KO mice
DOPAC	3,4-dihydroxyphenylacetic acid
DOPAL	3,4-dihydroxyphenylacetaldehyde
***Dyt1* d2KO mice**	D2R-expressing-cell-specific *Dyt1* conditional knockout mice

Author Manuscript Author Manuscript Author Manuscript Author Manuscript

D1R	dopamine receptor 1
D2R	dopamine receptor 2
***Dyt1* KI mice**	*Dyt1* ΔGAG heterozygous knock-in mice
FIHC	fluorescence immunohistochemistry
GAPDH	Glyceraldehyde-3-phosphate dehydrogenase
HACTV	horizontal activity
5-HIAA	5-hydroxyindoleacetic acid
5-HT	5-hydroxytryptamine: serotonin
HVA	homovanillic acid: 3-methoxy-4-hydroxyphenylacetic acid
KD	knock-down
KO	knock-out
LFTIME	left front time
LRTIME	left rear time
LTD	long-term depression
MAO	Monoamine oxidase
MOVNO	horizontal movement number
MOVTIME	horizontal movement time
MRGDIST	marginal distance
MRGTIME	marginal time
MSN	medium spiny neuron
3-MT	3-methoxytyramine
PB	phosphate buffer
RESTIME	rest time
PTX	picrotoxin
RFTIME	right front time
sEPSC	spontaneous excitatory post-synaptic currents
SNc	substantia nigra compacta
SNr	substantia nigra reticulata
STRCNT	stereotypic movement count

Author Manuscript Author Manuscript Author Manuscript Author Manuscript

SSAO	semicarbazide-sensitive amine oxidase
STRNO	stereotypic number
STRTIME	stereotypic movement time
TH	tyrosine hydroxylase
THP	trihexyphenidyl
TrkA	Tropomyosin receptor kinase A
TOTDIST	total distance
VAChT	vesicular acetylcholine transporter
VACTV	vertical activity
VMOVNO	vertical movement number
VTIME	vertical movement time
WT	wild type

References

Abercrombie ED, et al., 1990 Effects of L-dopa on extracellular dopamine in striatum of normal and 6-hydroxydopamine-treated rats. Brain Res. 525, 36–44. [PubMed: 2123121]

Albanese A, et al., 2013 Phenomenology and classification of dystonia: a consensus update. Mov Disord. 28, 863–73. [PubMed: 23649720]

Alvarez-Fischer D, et al., 2012 Prolonged generalized dystonia after chronic cerebellar application of kainic acid. Brain Res. 1464, 82–8. [PubMed: 22595488]

Asanuma K, et al., 2005 Decreased striatal D2 receptor binding in non-manifesting carriers of the DYT1 dystonia mutation. Neurology. 64, 347–9. [PubMed: 15668438]

Augood SJ, et al., 2002 Dopamine transmission in DYT1 dystonia: a biochemical and autoradiographical study. Neurology. 59, 445–8. [PubMed: 12177384]

Avanes A, et al., 2019 Darpp-32 and t-Darpp protein products of PPP1R1B: Old dogs with new tricks. Biochem Pharmacol. 160, 71–79. [PubMed: 30552871]

Beaulieu JM, Gainetdinov RR, 2011 The physiology, signaling, and pharmacology of dopamine receptors. Pharmacol Rev. 63, 182–217. [PubMed: 21303898]

Bergeron AL, et al., 2005 The final stage of cholinergic differentiation occurs below inner hair cells during development of the rodent cochlea. J Assoc Res Otolaryngol. 6, 401–15. [PubMed: 16228856]

Berse B, et al., 2005 Expression of high affinity choline transporter during mouse development in vivo and its upregulation by NGF and BMP-4 in vitro. Brain Res Dev Brain Res. 157, 132–40. [PubMed: 15885806]

Bonsi P, et al., 2019 RGS9–2 rescues dopamine D2 receptor levels and signaling in DYT1 dystonia mouse models. EMBO Mol Med. 11, e9283.

Breakefield XO, et al., 2008 The pathophysiological basis of dystonias. Nat Rev Neurosci. 9, 222–34. [PubMed: 18285800]

Calakos N, et al., 2010 Functional evidence implicating a novel TOR1A mutation in idiopathic, late-onset focal dystonia. J Med Genet. 47, 646–50. [PubMed: 19955557]

Cao BJ, Li Y, 2002 Reduced anxiety- and depression-like behaviors in Emx1 homozygous mutant mice. Brain Res. 937, 32–40. [PubMed: 12020859]

Author Manuscript Author Manuscript Author Manuscript Author Manuscript

Cao S, et al., 2010 Chemical enhancement of torsinA function in cell and animal models of torsion dystonia. Dis Model Mech. 3, 386–96. [PubMed: 20223934]

Carter RJ, et al., Motor Coordination and Balance in Rodents In: Crawley J, (Ed.), Current Protocols in Neuroscience. John Wiley & Sons, Inc., 2001, pp. 8.12.1–8.12.14.

Cif L, et al., 2010 Long-term follow-up of DYT1 dystonia patients treated by deep brain stimulation: an open-label study. Mov Disord. 25, 289–99. [PubMed: 20063427]

Da Cunha C, et al., 2008 Hemiparkinsonian rats rotate toward the side with the weaker dopaminergic neurotransmission. Behav Brain Res. 189, 364–72. [PubMed: 18328580]

Dang MT, et al., 2012 An anticholinergic reverses motor control and corticostriatal LTD deficits in Dyt1 DeltaGAG knock-in mice. Behav Brain Res. 226, 465–72. [PubMed: 21995941]

Dang MT, et al., 2005 Generation and characterization of Dyt1 DeltaGAG knock-in mouse as a model for early-onset dystonia. Exp Neurol. 196, 452–63. [PubMed: 16242683]

Dang MT, et al., 2006 Motor deficits and hyperactivity in Dyt1 knockdown mice. Neurosci Res. 56, 470–4. [PubMed: 17046090]

DeAndrade MP, et al., 2016 Electromyographic evidence in support of a knock-in mouse model of DYT1 Dystonia. Mov Disord. 31, 1633–1639. [PubMed: 27241685]

DeAndrade MP, et al., 2011 Characterization of Atp1a3 mutant mice as a model of rapid-onset dystonia with parkinsonism. Behav Brain Res. 216, 659–65. [PubMed: 20850480]

DeSimone JC, et al., 2017 Forebrain knock-out of torsinA reduces striatal free-water and impairs whole-brain functional connectivity in a symptomatic mouse model of DYT1 dystonia. Neurobiol Dis. 106, 124–132. [PubMed: 28673740]

Doheny D, et al., 2002 Clinical findings of a myoclonus-dystonia family with two distinct mutations. Neurology. 59, 1244–6. [PubMed: 12391355]

Eidelberg D, et al., 1998 Functional brain networks in DYT1 dystonia. Ann Neurol. 44, 303–12. [PubMed: 9749595]

Eskow Jaunarajs KL, et al., 2015 Striatal cholinergic dysfunction as a unifying theme in the pathophysiology of dystonia. Prog Neurobiol. 127–128, 91–107.

Fagan AM, et al., 1997 A role for TrkA during maturation of striatal and basal forebrain cholinergic neurons in vivo. J Neurosci. 17, 7644–54. [PubMed: 9315886]

Fernagut PO, et al., 2002 Subacute systemic 3-nitropropionic acid intoxication induces a distinct motor disorder in adult C57Bl/6 mice: behavioural and histopathological characterisation. Neuroscience. 114, 1005–17. [PubMed: 12379255]

Furukawa Y, et al., 2000 Striatal dopamine in early-onset primary torsion dystonia with the DYT1 mutation. Neurology. 54, 1193–5. [PubMed: 10720299]

Gaspar P, et al., 1995 D1 and D2 receptor gene expression in the rat frontal cortex: cellular localization in different classes of efferent neurons. Eur J Neurosci. 7, 1050–63. [PubMed: 7613610]

Giles LM, et al., 2008 Dystonia-associated mutations cause premature degradation of torsinA protein and cell-type-specific mislocalization to the nuclear envelope. Hum Mol Genet. 17, 2712–22. [PubMed: 18552369]

Gong S, et al., 2007 Targeting Cre recombinase to specific neuron populations with bacterial artificial chromosome constructs. J Neurosci. 27, 9817–23. [PubMed: 17855595]

Goodchild RE, et al., 2005 Loss of the dystonia-associated protein torsinA selectively disrupts the neuronal nuclear envelope. Neuron. 48, 923–32. [PubMed: 16364897]

Gordon KL, Gonzalez-Alegre P, 2008 Consequences of the DYT1 mutation on torsinA oligomerization and degradation. Neuroscience. 157, 588–95. [PubMed: 18940237]

Grundmann K, et al., 2007 Overexpression of human wildtype torsinA and human DeltaGAG torsinA in a transgenic mouse model causes phenotypic abnormalities. Neurobiol Dis. 27, 190–206. [PubMed: 17601741]

Grusser-Cornehls U, et al., 1999 Vermectomy enhances parvalbumin expression and improves motor performance in weaver mutant mice: an animal model for cerebellar ataxia. Neuroscience. 91, 315–26. [PubMed: 10336081]

Isik E, et al., 2018 Biallelic TOR1A mutations cause severe arthrogryposis: A case requiring reverse phenotyping. Eur J Med Genet.

Author Manuscript Author Manuscript Author Manuscript Author Manuscript

Jankovic J, 2006 Treatment of dystonia. Lancet Neurol. 5, 864–72. [PubMed: 16987733]

Leung JC, et al., 2001 Novel mutation in the TOR1A (DYT1) gene in atypical early onset dystonia and polymorphisms in dystonia and early onset parkinsonism. Neurogenetics. 3, 133–43. [PubMed: 11523564]

Liang CC, et al., 2014 TorsinA hypofunction causes abnormal twisting movements and sensorimotor circuit neurodegeneration. J Clin Invest. 124, 3080–92. [PubMed: 24937429]

Maltese M, et al., 2017 Abnormal striatal plasticity in a DYT11/SGCE myoclonus dystonia mouse model is reversed by adenosine A2A receptor inhibition. Neurobiol Dis. 108, 128–139. [PubMed: 28823931]

Maltese M, et al., 2014 Anticholinergic drugs rescue synaptic plasticity in DYT1 dystonia: role of M1 muscarinic receptors. Mov Disord. 29, 1655–65. [PubMed: 25195914]

Mandavilli BS, et al., 2000 DNA damage in brain mitochondria caused by aging and MPTP treatment. Brain Res. 885, 45–52. [PubMed: 11121528]

Martella G, et al., 2009 Impairment of bidirectional synaptic plasticity in the striatum of a mouse model of DYT1 dystonia: role of endogenous acetylcholine. Brain. 132, 2336–49. [PubMed: 19641103]

Moseley AE, et al., 2007 Deficiency in Na,K-ATPase alpha isoform genes alters spatial learning, motor activity, and anxiety in mice. J Neurosci. 27, 616–26. [PubMed: 17234593]

Munro CA, et al., 2006 Sex differences in striatal dopamine release in healthy adults. Biol Psychiatry. 59, 966–74. [PubMed: 16616726]

Napolitano F, et al., 2010 Dopamine D2 receptor dysfunction is rescued by adenosine A2A receptor antagonism in a model of DYT1 dystonia. Neurobiol Dis. 38, 434–45. [PubMed: 20227500]

Ng GY, et al., 1996 Dopamine D2 receptor dimers and receptor-blocking peptides. Biochem Biophys Res Commun. 227, 200–4. [PubMed: 8858125]

Ngun TC, et al., 2011 The genetics of sex differences in brain and behavior. Front Neuroendocrinol. 32, 227–46. [PubMed: 20951723]

Nisenbaum ES, et al., 1994 Contribution of a slowly inactivating potassium current to the transition to firing of neostriatal spiny projection neurons. J Neurophysiol. 71, 1174–89. [PubMed: 8201411]

Oleas J, et al., 2015 Rodent Models of Autosomal Dominant Primary Dystonia In: Movement Disorders: Genetics and Models (LeDoux MS, ed), pp483–505. Academic Press Elsevier, New York.

Oleas J, et al., 2013 Engineering animal models of dystonia. Mov Disord. 28, 990–1000. [PubMed: 23893455]

Ozelius LJ, et al., 1997 The early-onset torsion dystonia gene (DYT1) encodes an ATP-binding protein. Nat Genet. 17, 40–8. [PubMed: 9288096]

Page ME, et al., 2010 Cell-autonomous alteration of dopaminergic transmission by wild type and mutant (DeltaE) TorsinA in transgenic mice. Neurobiol Dis. 39, 318–26. [PubMed: 20460154]

Pappas SS, et al., 2015 Forebrain deletion of the dystonia protein torsinA causes dystonic- like movements and loss of striatal cholinergic neurons. Elife. 4, e08352.

Pappas SS, et al., 2018 A cell autonomous torsinA requirement for cholinergic neuron survival and motor control. Elife. 7, e36691.

Patel TD, et al., 2000 Development of sensory neurons in the absence of NGF/TrkA signaling in vivo. Neuron. 25, 345–57. [PubMed: 10719890]

Qi Z, et al., 2008 Computational systems analysis of dopamine metabolism. PLoS One. 3, e2444.

Ritz K, Gerrits MC, Foncke EM, van Ruissen F, van der Linden C, Vergouwen MD, Bloem BR, Vandenberghe W, Crols R, Speelman JD, Baas F, Tijssen MA, 2009 Myoclonus-dystonia: clinical and genetic evaluation of a large cohort. J Neurol Neurosurg Psychiatry. 80, 653–658. [PubMed: 19066193]

Rosin DL, et al., 1998 Immunohistochemical localization of adenosine A2A receptors in the rat central nervous system. J Comp Neurol. 401, 163–86. [PubMed: 9822147]

Sanchez-Ortiz E, et al., 2012 TrkA gene ablation in basal forebrain results in dysfunction of the cholinergic circuitry. J Neurosci. 32, 4065–79. [PubMed: 22442072]

Author Manuscript Author Manuscript Author Manuscript Author Manuscript

Sano H, et al., 2013 Signals through the striatopallidal indirect pathway stop movements by phasic excitation in the substantia nigra. J Neurosci. 33, 7583–94. [PubMed: 23616563]

Sciamanna G, et al., 2012 Cholinergic dysregulation produced by selective inactivation of the dystonia-associated protein torsinA. Neurobiol Dis. 47, 416–27. [PubMed: 22579992]

Sharma N, et al., 2005 Impaired motor learning in mice expressing torsinA with the DYT1 dystonia mutation. J Neurosci. 25, 5351–5. [PubMed: 15930383]

Shih JC, et al., 2011 Transcriptional regulation and multiple functions of MAO genes. J Neural Transm (Vienna). 118, 979–86. [PubMed: 21359973]

Song CH, et al., 2013 Subtle microstructural changes of the striatum in a DYT1 knock-in mouse model of dystonia. Neurobiol Dis. 54, 362–71. [PubMed: 23336980]

Song CH, et al., 2012 Functional analysis of dopaminergic systems in a DYT1 knock-in mouse model of dystonia. Neurobiol Dis. 48, 66–78. [PubMed: 22659308]

Surmeier DJ, et al., 2007 D1 and D2 dopamine-receptor modulation of striatal glutamatergic signaling in striatal medium spiny neurons. Trends Neurosci. 30, 228–35. [PubMed: 17408758]

Tanabe LM, et al., 2012 Genetic background modulates the phenotype of a mouse model of DYT1 dystonia. PLoS One. 7, e32245.

Threlfell S, et al., 2012 Striatal dopamine release is triggered by synchronized activity in cholinergic interneurons. Neuron. 75, 58–64. [PubMed: 22794260]

Torres GE, et al., 2004 Effect of torsinA on membrane proteins reveals a loss of function and a dominant-negative phenotype of the dystonia-associated DeltaE-torsinA mutant. Proc Natl Acad Sci U S A. 101, 15650–5. [PubMed: 15505207]

Trusel M, et al., 2015 Coordinated Regulation of Synaptic Plasticity at Striatopallidal and Striatonigral Neurons Orchestrates Motor Control. Cell Rep. 13, 1353–1365. [PubMed: 26549453]

Ungerstedt U, Arbuthnott GW, 1970 Quantitative recording of rotational behavior in rats after 6-hydroxy-dopamine lesions of the nigrostriatal dopamine system. Brain Res. 24, 485–93. [PubMed: 5494536]

Wakabayashi-Ito N, et al., 2011 Dtorsin, the Drosophila ortholog of the early-onset dystonia TOR1A (DYT1), plays a novel role in dopamine metabolism. PLoS One. 6, e26183.

Xu M, et al., 2015 Targeted ablation of cholinergic interneurons in the dorsolateral striatum produces behavioral manifestations of Tourette syndrome. Proc Natl Acad Sci U S A. 112, 893–8. [PubMed: 25561540]

Yokoi F, et al., 2013 Pre-synaptic release deficits in a DYT1 dystonia mouse model. PLoS One. 8, e72491.

Yokoi F, et al., 2015a Behavioral and electrophysiological characterization of Dyt1 heterozygous knockout mice. PLoS One. 10, e0120916.

Yokoi F, et al., 2006 Myoclonus, motor deficits, alterations in emotional responses and monoamine metabolism in epsilon-sarcoglycan deficient mice. J Biochem. 140, 141–6. [PubMed: 16815860]

Yokoi F, et al., 2011 Motor deficits and decreased striatal dopamine receptor 2 binding activity in the striatum-specific Dyt1 conditional knockout mice. PLoS One. 6, e24539.

Yokoi F, et al., 2012a Improved motor performance in Dyt1 DeltaGAG heterozygous knock-in mice by cerebellar Purkinje-cell specific Dyt1 conditional knocking-out. Behav Brain Res. 230, 389–98. [PubMed: 22391119]

Yokoi F, et al., 2015b Decreased dopamine receptor 1 activity and impaired motor-skill transfer in Dyt1 DeltaGAG heterozygous knock-in mice. Behav Brain Res. 279, 202–10. [PubMed: 25451552]

Yokoi F, et al., 2009 Increased c-fos expression in the central nucleus of the amygdala and enhancement of cued fear memory in Dyt1 DeltaGAG knock-in mice. Neurosci Res. 65, 228–35. [PubMed: 19619587]

Yokoi F, et al., 2008 Motor deficits and hyperactivity in cerebral cortex-specific Dyt1 conditional knockout mice. J Biochem. 143, 39–47. [PubMed: 17956903]

Yokoi F, et al., 2005 Exclusive paternal expression and novel alternatively spliced variants of epsilon-sarcoglycan mRNA in mouse brain. FEBS Lett. 579, 4822–8. [PubMed: 16099459]

Author Manuscript Author Manuscript Author Manuscript Author Manuscript

Yokoi F, et al., 2012b Abnormal nuclear envelope in the cerebellar Purkinje cells and impaired motor learning in DYT11 myoclonus-dystonia mouse models. Behav Brain Res. 227, 12–20. [PubMed: 22040906]

Yokoi F, et al., 2012c Abnormal nuclear envelopes in the striatum and motor deficits in DYT11 myoclonus-dystonia mouse models. Hum Mol Genet. 21, 916–25. [PubMed: 22080833]

Yokoi F, et al., 2010 Earlier onset of motor deficits in mice with double mutations in Dyt1 and Sgce. J Biochem. 148, 459–66. [PubMed: 20627944]

Zawarynski P, et al., 1998 Dopamine D2 receptor dimers in human and rat brain. FEBS Lett. 441, 383–6. [PubMed: 9891976]

Zhang Y, et al., 2000 Cell surface Trk receptors mediate NGF-induced survival while internalized receptors regulate NGF-induced differentiation. J Neurosci. 20, 5671–8. [PubMed: 10908605]

Zhao Y, et al., 2008 Abnormal motor function and dopamine neurotransmission in DYT1 DeltaGAG transgenic mice. Exp Neurol. 210, 719–30. [PubMed: 18299128]

Zucca S, et al., 2018 Pauses in cholinergic interneuron firing exert an inhibitory control on striatal output in vivo. Elife. 7, e32510.

Author Manuscript Author Manuscript Author Manuscript Author Manuscript

Highlights

- *Dyt1* d2KO mice had motor deficits in rotarod and beam-walking without overt dystonia.
- *Dyt1* d2KO mice had a reduced number of striatal cholinergic interneurons.
- *Dyt1* d2KO mice exhibited a reduced level of striatal dopamine receptor 2 dimer.
- *Dyt1* d2KO mice exhibited a reduced level of striatal tyrosine hydroxylase.
- *Dyt1* d2KO mice showed a correlation between striatal monoamines and locomotion.

Author Manuscript Author Manuscript Author Manuscript Author Manuscript

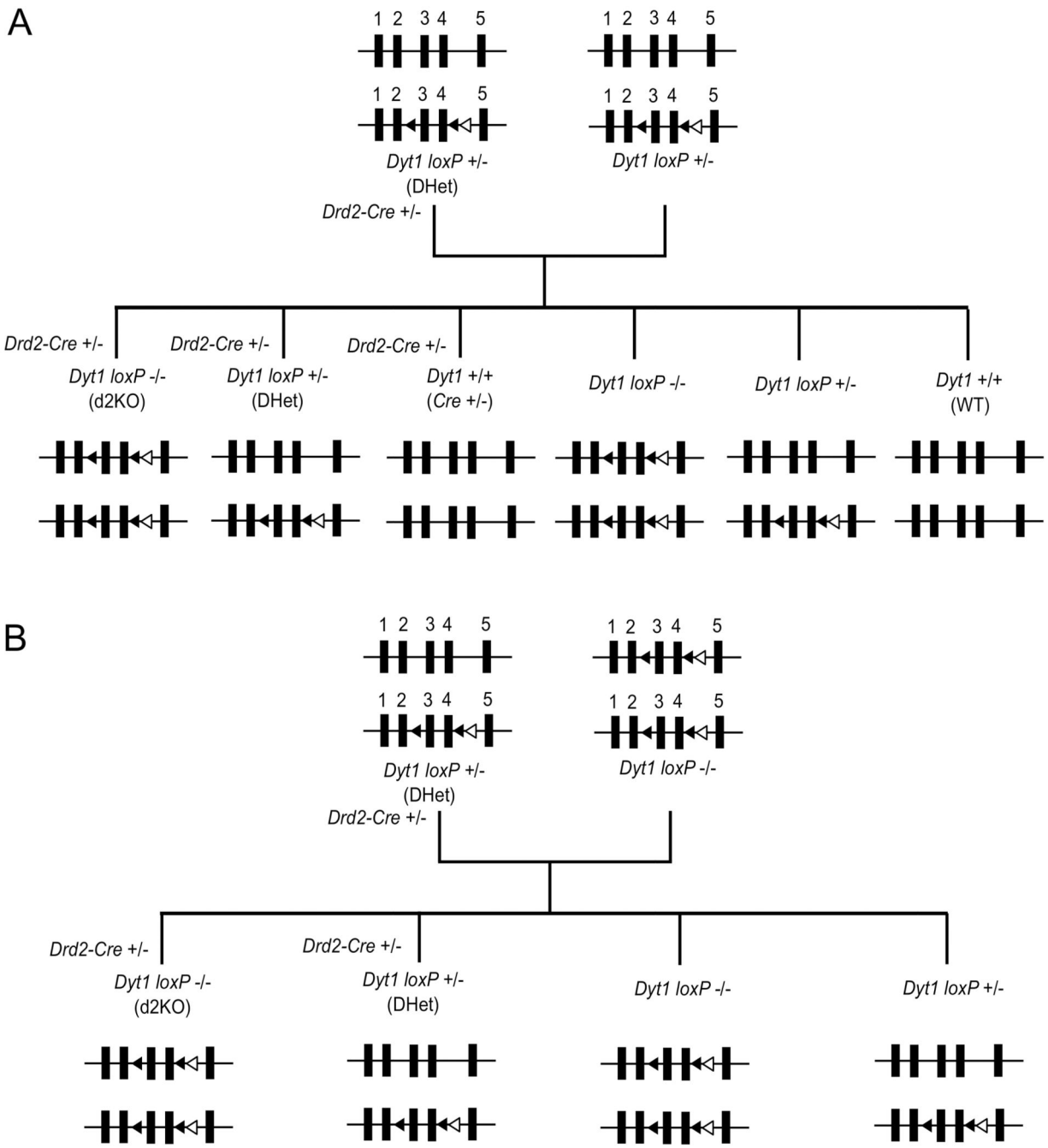

Fig. 1.

(A) Breeding scheme to generate *Dyt1* d2KO mice. *Drd2-Cre* +/− *Dyt1 loxP* +/− (DHet) mice were crossed with *Dyt1 loxP* +/− mice to generate *Drd2-Cre* +/− *Dyt1 loxP* −/− (d2KO), *Drd2- Cre* +/− *Dyt1 loxP* +/− (DHet), *Drd2-Cre* +/− (*Cre* +/−), *Dyt1 loxP* −/−, *Dyt1 loxP* +/−, and *Dyt1 loxP* +/+ (WT) mice. (B) Another breeding scheme to generate *Dyt1* d2KO mice. *Drd2-Cre* +/− *Dyt1 loxP* +/− (DHet) mice were also crossed with *Dyt1 loxP* −/− mice to generate *Drd2-Cre* +/− *Dyt1 loxP* −/− (d2KO), *Drd2-Cre* +/− *Dyt1 loxP* +/− (DHet),

Author Manuscript Author Manuscript Author Manuscript Author Manuscript

Dyt1 loxP −/−, and *Dyt1 loxP* +/− mice. Notations; *Dyt1* + and *Dyt1 loxP* +: wild-type of *Dyt1* (*Tor1a*) allele; *Dyt1 loxP* -: floxed *Dyt1* allele, before conditionally knocked-out.

Author Manuscript
Author Manuscript
Author Manuscript
Author Manuscript

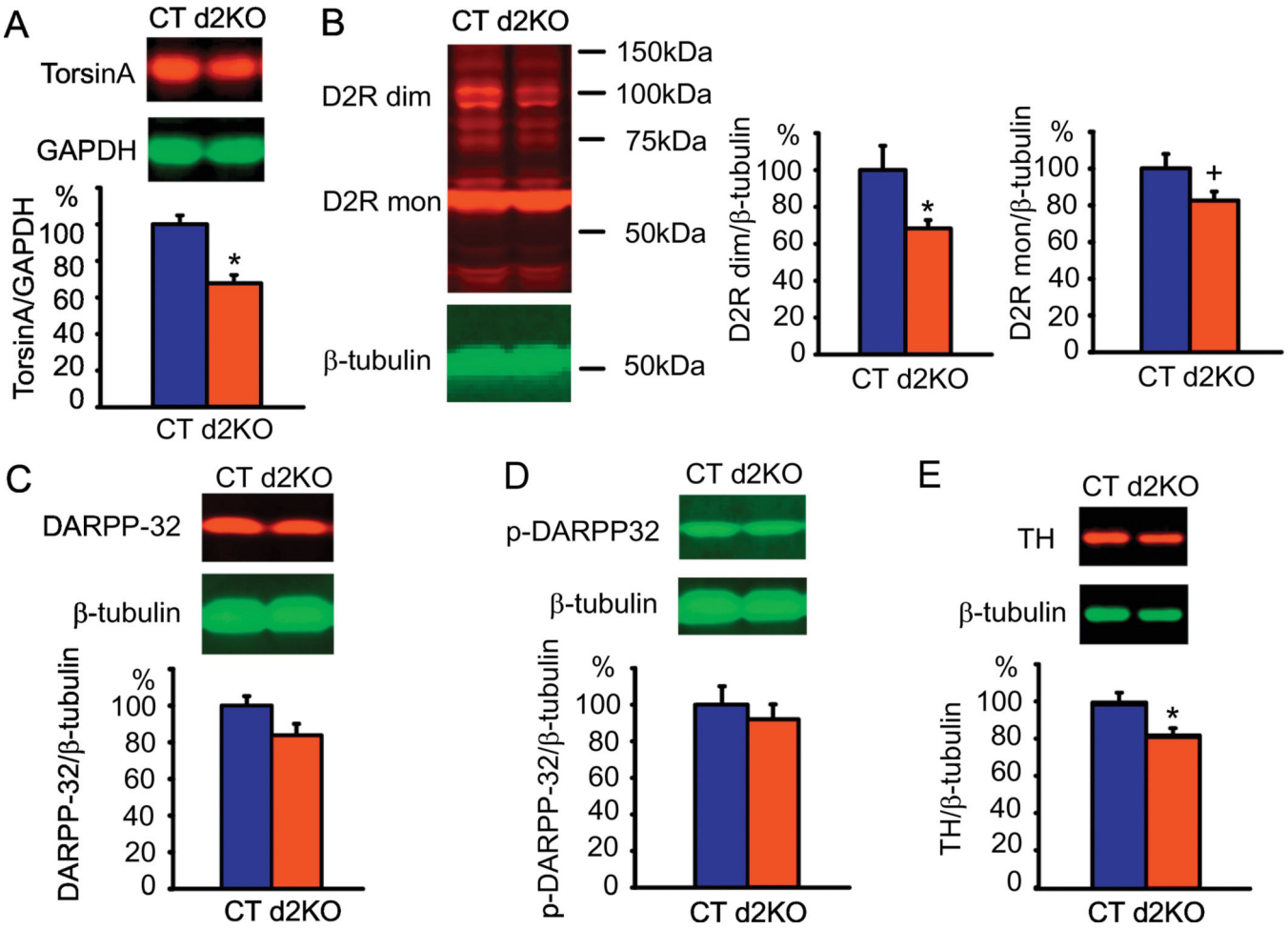

Fig. 2.

Representative western blot images and their quantifications (bar graphs) of the striatal tissue samples. (A) *Dyt1* d2KO mice showed a significant reduction of the torsinA/GAPDH level. (B) *Dyt1* d2KO mice showed a significant reduction of D2R dimer (dim)/β-tubulin and a trend of reduction of D2R monomer (mon)/β-tubulin level. (C) *Dyt1* d2KO mice did not show a significant difference in DARPP-32/β-tubulin level. (D) *Dyt1* d2KO mice did not show a significant difference in phosphorylated DARPP-32/β-tubulin level. (E) *Dyt1* d2KO mice showed a significant reduction of the striatal TH/β-tubulin level. The bar graphs show mean ± standard errors. $+p < 0.1$, $*p < 0.05$.

Author Manuscript Author Manuscript Author Manuscript Author Manuscript

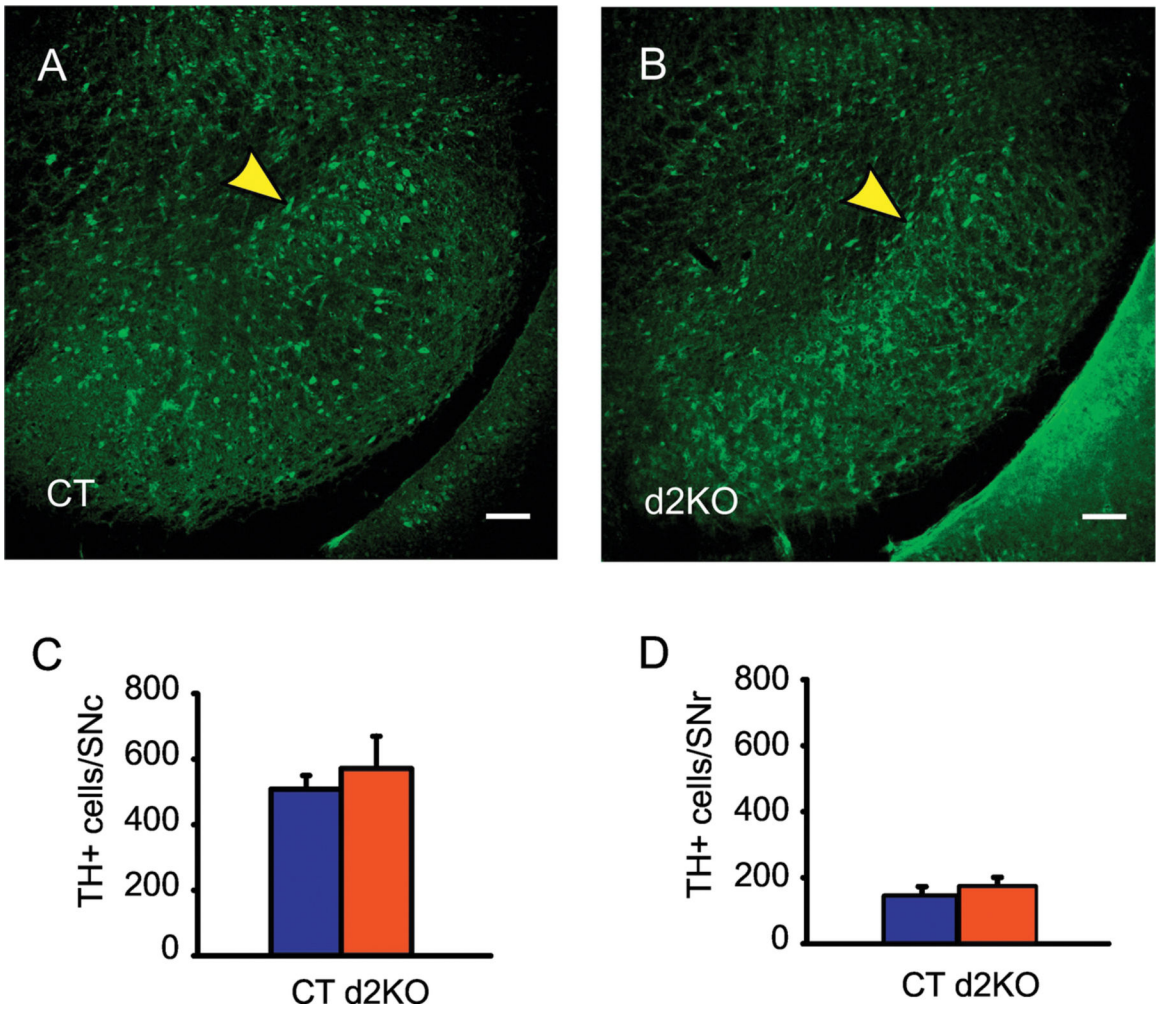

Fig. 3.

(A) A representative fluorescence immunohistochemistry image of the TH-positive dopaminergic neurons in the substantia nigra of a *Dyt1 loxP* −/− mouse as a control (CT). (B) A representative fluorescence immunohistochemistry image of the TH-positive dopaminergic neurons in the substantia nigra of a *Dyt1* d2KO mouse (d2KO). The yellow arrowheads indicate the TH-positive cells in SNc. Scale bar indicates 100 μm. (C) Quantification of the density of TH- positive dopaminergic neurons in the SNc (neurons/mm^2). (D) Quantification of the density of TH-positive dopaminergic neurons in the SNr (neurons/mm^2). The bar graphs indicate the means ± standard errors.

Author Manuscript Author Manuscript Author Manuscript Author Manuscript

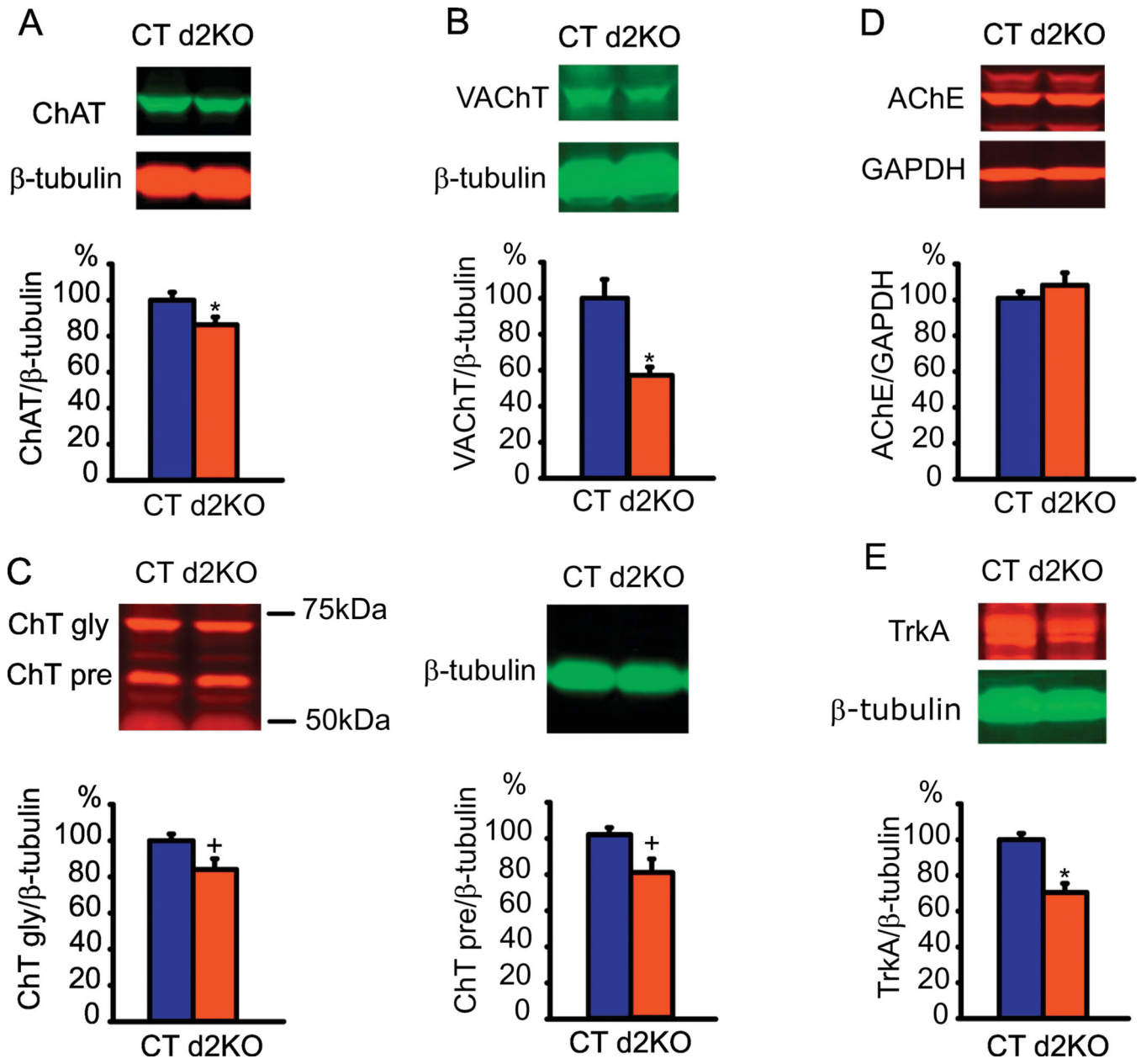

Fig. 4.

Representative Western blot images (top) and their quantifications (bottom) of the striatal tissue samples. *Dyt1* d2KO mice showed significant reductions of the striatal ChAT/β-tubulin (A) and VAChT/β-tubulin (B). *Dyt1* d2KO mice also showed a trend of reduction in both the glycosylated form (gly) and premature form (pre) of ChTs/β-tubulin (C). On the other hand, *Dyt1* d2KO mice did not show a significant difference in AChE/GAPDH level (D). *Dyt1* d2KO mice showed a significant reduction of the TrkA/GAPDH (E). The bar graphs show mean ± standard errors. $+p < 0.1$, $*p < 0.05$.

Author Manuscript Author Manuscript Author Manuscript Author Manuscript

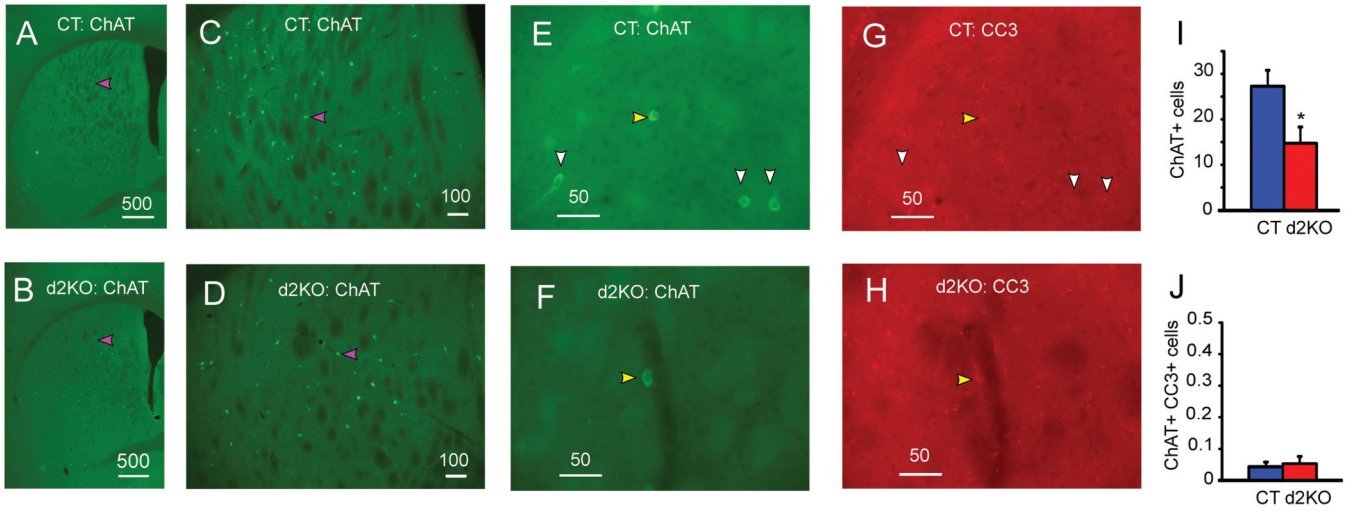

Fig. 5.

Representative images of the fluorescence immunohistochemistry (FIHC) and quantified densities of ChAT-positive and ChAT-, CC3-double-positive striatal ChIs. (A) Striatum stained with ChAT antibody and taken by using × 2 objective lens in CT (A) and d2KO (B). Enlarge images of the same slices taken by using × 10 objective lens; CT (C) and d2KO (D). Enlarge images of another set of slices double-stained with ChAT (CT: E, d2KO: F) and CC3 antibodies (CT: G, d2KO: H) and taken by using × 40 objective lens. (I) The quantified densities of the striatal ChIs (ChAT-positive cell numbers/mm^2). *Dyt1* d2KO mice showed a significant reduction of striatal ChIs. (J) The quantified densities of CC3-positive striatal ChIs (ChAT and CC3 double-positive cell numbers/mm^2). CC3-positive striatal ChIs were very rare and there was no significant difference between CT and *Dyt1* dKO mice. Pink arrowheads show the representative striatal ChIs stained with ChAT antibody (A-D). Yellow arrowheads show the representative both ChAT-positive (E, F) and CC3-positive (G, H) striatal ChIs in the double- staining FIHC. White arrowheads show the representative ChAT-positive (E), CC3-negative (G) striatal ChIs in the double-staining FIHC. Scale bars indicate 500 μm (A, B), 100 μm (C, D), or 50 μm (E–H). The bar graphs show means ± standard errors (I, J). *$p < 0.05$.

Author Manuscript Author Manuscript Author Manuscript Author Manuscript

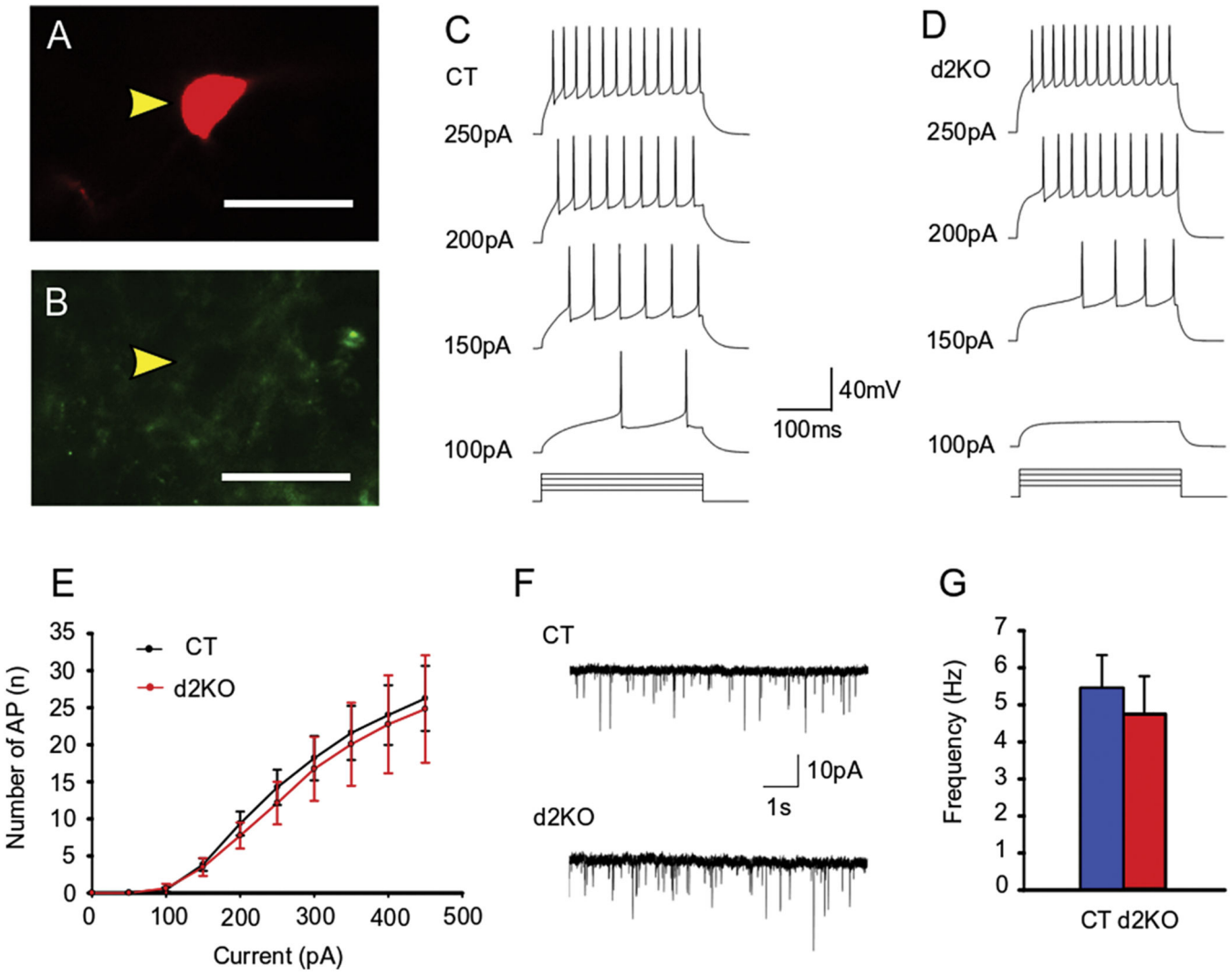

Fig. 6.

Electrophysiological properties of the striatal indirect pathway MSNs in d2KO mice. (A) A representative histochemical image of the recorded brain slice stained with streptavidin Alexa Fluor 594 conjugate through biocytin-streptavidin binding to identify the recorded MSN. Arrowhead indicates the recorded neuron. (B) Histochemical identification of the striatal indirect pathway MSNs. A representative immunohistochemical image of the same slice stained with anti-A2A antibody and Alexa Fluor 488-conjugated secondary antibody to identify the striatal indirect pathway MSNs. Arrowhead indicates the stained A2A at the cellular membrane of the recorded indirect pathway MSN. Scale bars indicate 25 μm in (A) and (B). (C, D) Representative trances of the action potentials evoked by step-current injection in whole-cell current-clamp mode. Representative responses to each current injection (pA at the left) are shown for CT (C) and d2KO mice (D). The bottom figure shows the representative current injection (100–250pA) used for the corresponding trances. (E) The frequency-current relationship of the striatal MSNs (CT: n=11; dKO: n=18). There was no significant difference in the number of evoked action potential (AP) in each current step injection. (F) Representative trances of the sEPSCs recorded in whole-cell voltage-clamp

mode. (G) Frequency of the sEPSCs. There is no significant difference between CT and d2KO mice. Means ± standard errors are shown in E and G.

Author Manuscript Author Manuscript Author Manuscript Author Manuscript

Author Manuscript Author Manuscript Author Manuscript Author Manuscript

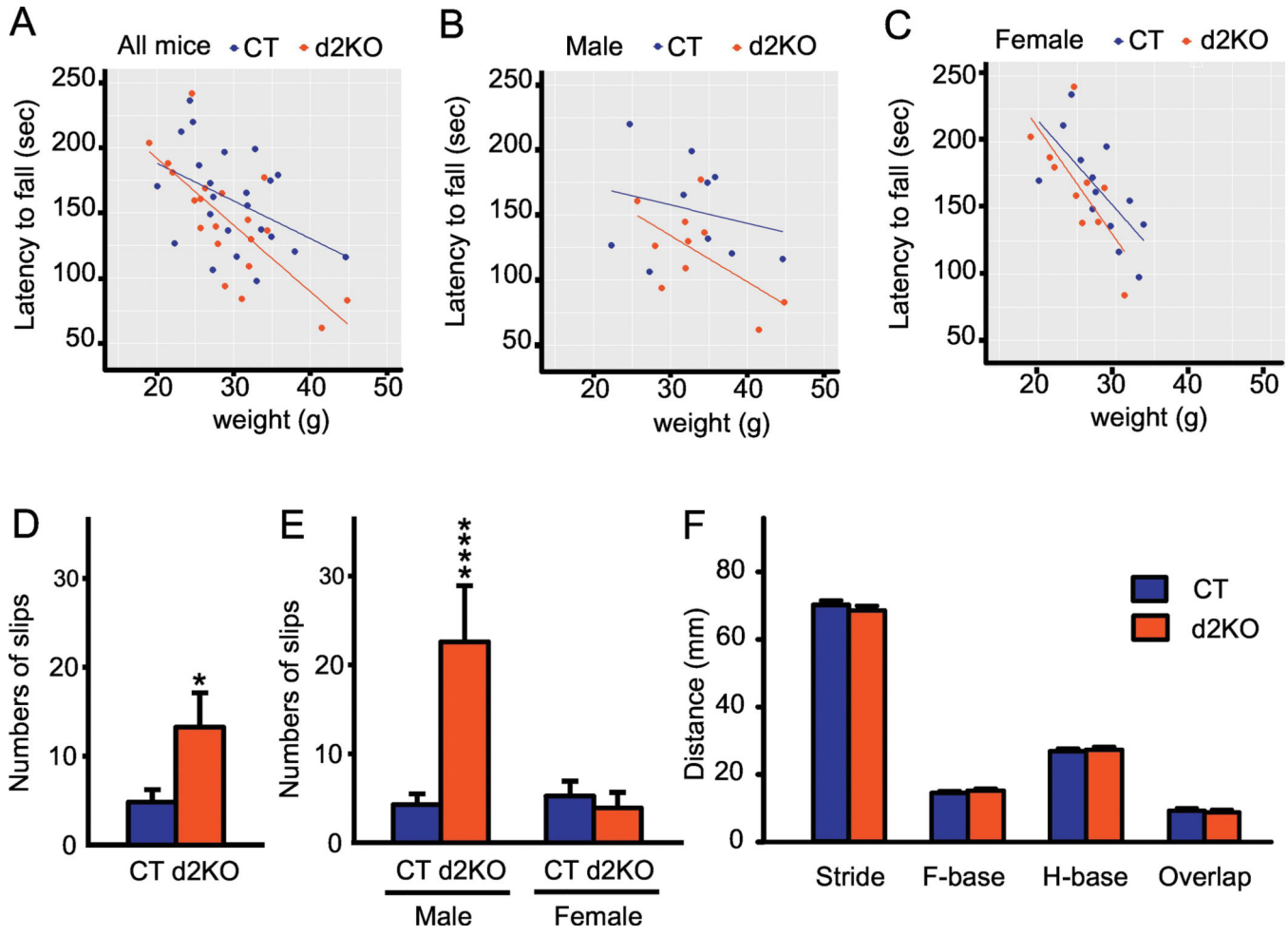

Fig. 7.

Motor performance of *Dyt1* d2KO mice. (A) In the accelerated rotarod test, there was a trend of decreased latency to fall of d2KO mice but no significant difference in the averaged latency to fall between CT (n=23) and d2KO mice (n=20). (B) *Dyt1* d2KO male mice (n=10) showed a significantly decreased latency to fall than CT male mice (n=10). (C) There was no significant difference in the latency to fall between CT (n=13) and *Dyt1* d2KO female mice (n=10). (D) In the beam-walking test, *Dyt1* d2KO mice showed a significant increase in slip numbers. (E) *Dyt1* d2KO male mice showed a significant increase of total slip numbers, On the other hand, there was no significant difference in slip numbers between CT and *Dyt1* d2KO female mice. (F) In paw-print test, *Dyt1* d2KO mice didn't show significant difference in the stride, fore-base (F-base), hind-base (H-base), or overlap. *$p <$ 0.05, ****$p < 0.0001$.

Author Manuscript

Author Manuscript

Author Manuscript

Author Manuscript

Table 1.

Electrophysiological membrane properties of the striatal indirect pathway MSNs

Membrane properties	CT (16 cells/5 mice)	d2KO (8 cells/3 mice)	*p*
Cm (pF)	40.63 ± 4.21	51.19 ± 5.48	0.829
Rm (MΩ)	202.83 ± 19.12	219.17 ± 29.15	0.041 *
Tau (ms)	0.86 ± 0.12	0.88 ± 0.16	0.924
MP (mV)	−90.10 ± 1.19	−88.91 ± 1.55	0.557

Cm: Capacitance; Rm: membrane resistance; Tau: Time constant; MP: resting membrane potential; SAS mixed procedure was used to calculate p-values for Cm, Tau and MP with a normal distribution. SAS GENMOD procedure was used to calculate p-values for Rm with log link and gamma distribution. Nested data in each mouse were used for the analysis. Means ± standard errors are shown.

* $p<0.05$.

Author Manuscript

Author Manuscript

Author Manuscript

Author Manuscript

Table 2.

Action potentials evoked by a step-current in the striatal indirect pathway MSNs

Evoked action potential	CT (16 cells/5 mice)	d2KO (8 cells/3 mice)	*p*
Amplitude (mV)	44.36 ± 3.45	52.34 ± 4.90	0.20
Rise (ms)	2.02 ± 0.06	1.99 ± 0.09	0.78
Decay (ms)	1.18 ± 0.07	1.16 ± 0.10	0.90
Area (mVms)	69.52 ± 5.11	77.29 ± 7.25	0.39

The kinetics parameters of the action potentials evoked by a step current (400pA) were analyzed. SAS mixed procedure was used to calculate *p*-values for the nested data in each mouse with a normal distribution. Means ± standard errors are shown.

Author Manuscript

Author Manuscript

Author Manuscript

Author Manuscript

Table 3.

sEPSCs in the striatal indirect pathway MSNs

sEPSC	CT (16 cells/5 mice)	d2KO (8 cells/3 mice)	*p*
Amplitude (pA)	7.23 ± 0.54	8.24 ± 0.77	0.30
Rise (ms)	2.43 ± 0.13	2.35 ± 0.18	0.73
Decay (ms)	4.07 ± 0.28	3.82 ± 0.40	0.63
Area (pAms)	33.32 ± 3.57	36.32 ± 5.08	0.64

The kinetics parameters of the sEPSCs are shown. SAS mixed procedure was used to calculate *p*-values for the nested data in each mouse with a normal distribution. Means ± standard errors are shown.

Author Manuscript
Author Manuscript
Author Manuscript
Author Manuscript

Table 4.

Neurochemicals in the striatal tissues

Content or ratio	CT	d2KO	*p*
DA	64.62 ± 4.35	70.50 ± 6.76	0.471
DOPAC	4.42 ± 0.28	4.54 ± 0.38	0.790
HVA	8.94 ± 0.51	9.14 ± 0.66	0.811
3-MT	3.44 ± 0.26	4.07 ± 0.45	0.237
Noradrenaline	2.64 ± 0.28	2.95 ± 0.33	0.480
5-HT	8.04 ± 0.45	8.58 ± 0.40	0.373
5-HIAA	6.20 ± 0.31	6.83 ± 0.33	0.173
DOPAC/DA	0.069 ± 0.001	0.067 ± 0.002	0.202
HVA/DA	0.143 ± 0.004	0.138 ± 0.005	0.491
3-MT/DA 5-HIAA/5-HT	0.056 ± 0.005 0.800 ± 0.044	0.058 ± 0.004 0.807 ± 0.035	0.720 0.898

The striatal neurochemicals were compared between CT (n=23) and *Dyt1* d2KO (n=20) mice by Welch's t-test. The values of neurochemicals are shown as means ± standard errors (in ng/mg protein). The turnovers of metabolites are also shown as the ratios of the corresponding neurochemicals. DA (dopamine), DOPAC (3,4-dihydroxyphenylacetic acid), HVA (homovanillic acid: 3-methoxy-4-hydroxyphenylacetic acid), 3-MT (3-methoxytyramine), 5-HT (serotonin), 5- HIAA (5-hydroxyindoleacetic acid).

Author Manuscript

Author Manuscript

Author Manuscript

Author Manuscript

Table 5.

The striatal neurochemicals in each sex

Content or ratio	Male CT	Male d2KO	*p*	Female CT	Female d2KO	*p*
DA	68.08 ± 6.50	61.69 ± 10.46	0.611	61.96 ± 5.98	79.30 ± 8.15	0.104
DOPAC	4.58 ± 0.43	4.03 ± 0.57	0.449	4.29 ± 0.37	5.05 ± 0.49	0.229
HVA	8.98 ± 0.69	8.39 ± 1.07	0.652	8.90 ± 0.75	9.88 ± 0.76	0.371
3-MT	3.44 ± 0.44	2.94 ± 0.51	0.460	3.45 ± 0.33	5.21 ± 0.56	0.016 *
Noradrenaline	3.11 ± 0.58	3.66 ± 0.51	0.490	2.27 ± 0.20	2.24 ± 0.32	0.938
5-HT	9.08 ± 0.83	8.84 ± 0.62	0.819	7.24 ± 0.36	8.32 ± 0.53	0.111
5-HIAA	5.53 ± 0.51	6.37 ± 0.50	0.258	6.72 ± 0.32	7.29 ± 0.41	0.285
DOPAC/DA	0.067 ± 0.002	0.069 ± 0.003	0.687	0.071 ± 0.002	0.064 ± 0.002	0.031 *
HVA/DA	0.134 ± 0.004	0.146 ± 0.008	0.204	0.149 ± 0.007	0.129 ± 0.007	0.051 +
3-MT/DA	0.051 ± 0.005	0.049 ± 0.003	0.739	0.060 ± 0.008	0.068 ± 0.006	0.452
5-HIAA/5-HT	0.615 ± 0.021	0.721 ± 0.020	0.002 **	0.942 ± 0.045	0.893 ± 0.057	0.508

The striatal neurochemicals were compared between CT and *Dyt1* d2KO mice in each sex separately by Welch's t-test. The values of neurochemicals in male CT (n=10), male *Dyt1* d2KO (n=10), female CT (n=13), and female *Dyt1* d2KO (n=10), are shown as means ± standard errors (in ng/mg protein). The turnovers of metabolites are also shown as the ratios of the corresponding neurochemicals. DA (dopamine), DOPAC (3,4-dihydroxyphenylacetic acid), HVA (homovanillic acid: 3-methoxy-4-hydroxyphenylacetic acid), 3-MT (3-methoxytyramine), 5-HT (serotonin), 5-HIAA (5-hydroxyindoleacetic acid).

$^{+}p < 0.1$

$^{*}p < 0.05$

$^{**}p < 0.01$.

Author Manuscript Author Manuscript Author Manuscript Author Manuscript

Table 6.

Correlations between striatal neurochemicals and spontaneous locomotor activities in the open-field test.

	CT (n=23)		d2KO(n=20)	
Compared subjects	**PCC**	***p***	**PPC**	***p***
HIAA:VTIME	−0.40745	0.048 *	−0.12294	0.606
Noradrenaline:STRCNT	−0.04039	0.851	−0.45165	0.046 *
Noradrenaline:STRTIME	0.03116	0.885	−0.4733	0.035 *
DOPAC/DA:HACTV	0.05217	0.809	−0.59716	0.005 **
DOPAC/DA:TOTDIST	0.07187	0.739	−0.59577	0.006 **
DOPAC/DA:MOVNO	−0.03465	0.872	−0.49292	0.027 *
DOPAC/DA:MOVTIME	0.03269	0.880	−0.59599	0.006 **
DOPAC/DA:RESTIME	−0.03233	0.880	0.59625	0.006 **
DOPAC/DA:MRGTIME	−0.0326	0.880	0.46027	0.041 *
DOPAC/DA:CTRDIST	0.00045	0.998	−0.59086	0.006 **
DOPAC/DA:CTRTIME	0.0326	0.880	−0.46027	0.041 *
DOPAC/DA:ACWREV	0.22826	0.283	−0.73274	0.0002 ***
HVA/DA:HACTV	−0.0912	0.672	−0.53768	0.015 *
HVA/DA:TOTDIST	−0.14649	0.495	−0.45271	0.045 *
HVA/DA:ACWREV	−0.01715	0.937	−0.55731	0.011 *
HVA/DA:CTRDIST	−0.10866	0.613	−0.52251	0.018 *
DA:HACTV	0.06368	0.768	0.46256	0.040 *
DA:CTRDIST	0.07153	0.740	0.46881	0.037 *

PPC: Pearson Correlation Coefficients; VTIME: vertical movement time; STRCNT: stereotypic movement number; STRTIME: stereotypic movement time; HACTV: horizontal activity; TOTDIST: total distance; MOVNO: horizontal movement number; MOVTIME: horizontal movement time; RESTIME: rest time; MRGTIME: marginal time; CTRDIST; central distance: CTRTIME: central time; ACWREV: anticlockwise revolutions

* $p<0.05$

** $p<0.01$

*** $p<0.001$.

Author Manuscript Author Manuscript Author Manuscript Author Manuscript

Table 7.

Correlations in each sex among striatal neurochemicals and spontaneous locomotor activities

Content or ratio	M CT	*p*	M d2KO	*p*	F CT	*p*	F d2KO	*p*
Noradrenaline:STRCNT	−0.12206	0.7943	−0.94497	0.0044**	−0.23554	0.4385	0.30578	0.3902
Noradrenaline:STRNO	0.32647	0.4748	−0.93903	0.0054**	−0.27572	0.3618	0.22680	0.5286
Noradrenaline:STRTIME	0.28260	0.5391	−0.96382	0.0019**	0.04344	0.8879	−0.00941	0.9794
DOPAC/DA:HACTV	0.11327	0.8089	−0.97996	0.0005***	−0.07029	0.8194	−0.03596	0.9214
DOPAC/DA:VMOVNO	−0.71603	0.0703	−0.94587	0.0043**	−0.46504	0.1093	−0.08332	0.8190
DOPAC/DA:STRCNT	0.61063	0.1452	−0.94471	0.0045**	0.03024	0.9218	−0.00808	0.9823
DOPAC/DA:STRNO	0.88179	0.0086**	−0.65057	0.1618	−0.02649	0.9315	0.16686	0.6449
5-HIAA:CTRTIME	−0.25294	0.5842	−0.92994	0.0071**	0.09629	0.7543	−0.19579	0.5877
3-HVA/DA:HACTV	−0.33175	0.4672	−0.94534	0.0043**	0.01166	0.9698	0.09222	0.7999
3-HVA/DA:VMOVNO	−0.40990	0.3610	−0.91723	0.0099**	−0.38672	0.1917	−0.41555	0.2323
3-HVA/DA:STRCNT	0.13895	0.7663	−0.96845	0.0014**	0.20908	0.4930	0.13577	0.7084
5-HT:ACWREV	−0.03437	0.9416	−0.39494	0.4383	−0.73400	0.0042**	0.19978	0.5800
3-MT:HACTV	0.83482	0.0194*	0.92188	0.0089**	0.28274	0.3492	−0.25412	0.4786
3-MT:STRCNT	0.36880	0.4156	0.92147	0.0090**	0.12388	0.6867	−0.18444	0.6099
3-MT:CWREV	0.88662	0.0078**	0.67199	0.1437	0.33455	0.2638	0.03548	0.9224
3-MT/DA:CWREV	0.89103	0.0070**	0.21639	0.6804	−0.17517	0.5670	−0.17780	0.6231

Correlations among the striatal neurochemicals and spontaneous movements were compared between male control (M CT; n=10), male *Dyt1* d2KO (M d2KO; n=10), female control (F CT; n=13), and female *Dyt1* d2KO (F d2KO; n=10) mice.

* $p < 0.05$

** $p < 0.01$

*** $p < 0.001$.